circFAM73A Promotes Cancer Stem Cell-like Properties of Gastric Cancer Through miR-490-3p/HMGA2 Positive Feedback and HNRNPK-mediated β-catenin Stabilization.

Yiwen Xia
Jiangsu Province Hospital and Nanjing Medical University First Affiliated Hospital
Jialun Lv
Jiangsu Province Hospital and Nanjing Medical University First Affiliated Hospital
Tianlu Jiang
Jiangsu Province Hospital and Nanjing Medical University First Affiliated Hospital
Bowen Li
Jiangsu Province Hospital and Nanjing Medical University First Affiliated Hospital
Zhongyuan He
Jiangsu Province Hospital and Nanjing Medical University First Affiliated Hospital
Zhe Xuan
Jiangsu Province Hospital and Nanjing Medical University First Affiliated Hospital
Guangli Sun
Jiangsu Province Hospital and Nanjing Medical University First Affiliated Hospital
Sen Wang
Jiangsu Province Hospital and Nanjing Medical University First Affiliated Hospital
Zheng Li
Jiangsu Province Hospital and Nanjing Medical University First Affiliated Hospital
Weizhi Wang
Jiangsu Province Hospital and Nanjing Medical University First Affiliated Hospital
Linjun Wang
Jiangsu Province Hospital and Nanjing Medical University First Affiliated Hospital
Zekuan Xu (xuzekuan8321@163.com)
Department of General Surgery, The First Affiliated Hospital of Nanjing Medical University, No.300, Guangzhou Road, Nanjing, Jiangsu Province, China

---

Research

Keywords: circRNAs, Cancer stem cell, Gastric cancer, HMGA2

Posted Date: November 4th, 2020

DOI: https://doi.org/10.21203/rs.3.rs-100290/v1

Version of Record: A version of this preprint was published on March 17th, 2021. See the published version at https://doi.org/10.1186/s13046-021-01896-9.

Abstract

Background: Circular RNAs (circRNAs) have emerged as a new subclass of regulatory RNAs that exert critical roles in various cancers. Cancer stem cells (CSCs), a small subset of cancer cells, are believed to possess the capacities to initiate tumorigenesis and promote progression. Although accumulating evidences have suggested that cells with CSC-like properties are crucial for the malignance process of gastric cancer (GC), it remains inexplicit whether circRNAs are interrelated with the acquisition of CSC-like properties in GC.

Methods: circFAM73A expression was analyzed by GEO datasets and verified in GC samples. The role of circFAM73A on GC cell proliferation, migration, cisplatin resistance and CSC-like properties were determined by a series of functional experiment both *in vitro* and *in vivo*. RNA pull down was used to explore the miRNAs and proteins binding to circFAM73A. Bioinformatic analysis and experimental verification confirmed the downstream of circFAM73A. The regulation of HMGA2 on circFAM73A was verified by ChIP and RIP assays.

Results: Elevated circFAM73A expression was confirmed in GC tissues and higher circFAM73A predicts poor prognosis of GC patients. The upregulation of circFAM73A enhanced CSC-like properties in GC, thus, exerting the facilitating role on cell proliferation, migration and cisplatin resistance. Mechanistically, circFAM73A promoted GC malignancy by regulating miR-490-3p/HMGA2 in a positive feedback loop and recruiting HNRNPK to facilitate β-catenin stabilization. Moreover, HMGA2 further enhanced E2F1 and HNRNPL activity, which in turn promotes circFAM73A expression.

Conclusions: Our work demonstrates the crucial role of circFAM73A on GC CSC-like properties and uncovers a positive feedback loop on circFAM73A regulation that leads to the progression of gastric cancer, which may provide a new insight for circRNA-based diagnostic and therapeutic strategies.

Background

Gastric cancer (GC) remains one of the most frequently diagnosed cancer and is responsible for over 1,000,000 new cases and an approximated 783,000 deaths annually, making it the fifth common cancer and ranks as the third leading cause of cancer-associated mortality worldwide[1]. Therefore, novel effective strategies of diagnosis and therapeutic are in urgent demand.

Cancer stem cells (CSCs) are defined as the fraction of cells that retains the capacities of self-renewal and differentiation[2]. Although CSCs only account for a small proportion in cancer cells, they exhibit prominent features including tumorigenesis, chemotherapy resistance and high metastatic potential, which have been shown to be largely responsible for cancer metastasis, recurrence and treatment failure[3, 4]. Emerging evidence have supported the existence of CSCs in GC, where they were isolated based on the expression of CSC-specific surface markers[5, 6]. Nevertheless, the underlying regulatory mechanism of CSCs in GC remains to be elucidated.

Circular RNA (circRNA) is a widespread special form of RNA, which is mostly generated from back-splicing of precursor mRNA (pre-mRNA)[7, 8]. Despite identification of circular RNA dating back to the mid-1970s[9], these transcripts had largely been assumed to be aberrant splicing byproducts and thus remained under-researched[10, 11]. With the rapid growth of next-generation profiling of non-coding RNAs, however, the simplistic view of circRNA as transcriptional noise has given way to a deeper understanding of its various biological function. CircRNAs are now speculated to be highly conserved and stable as the circular structures resists to most RNA decay mechanisms[12, 13]. Mounting evidence implicates the involvement of cirRNAs in several physiological and pathological processes[14–16], including cancer[17–20]. Therefore, cirRNAs may also serve as potential biomarkers in many malignancies[17, 21, 22]. However, little is known about the overall pathophysiological effects of circRNAs on stem cell-like properties.

Here, we set out to investigate whether circRNA involves in the CSC-like properties in GC. Our findings demonstrate that circFAM73A promotes gastric cancer stem cell-like properties, thus augments GC cell malignance in GC. More importantly, elevated circFAM73A predicts poor prognosis in GC patients. circFAM73A regulates HMGA2 expression by absorbing miR-490-3p, while HMGA2 facilitates the transcriptional activation of FAM73A by E2F1 and enhances the efficiency of cirFAM73A circularization by HNRNPL, which forms a positive feedback to further elevate circFAM73A expression. Besides, circFAM73A also recruits HNRNPK, enhances the interaction between HNRNPK and β-catenin and facilitates the stability of β-catenin.

Hence, our study uncovers a novel mechanism of circFAM73A that prompts GC progression and demonstrates the intrinsic value of circFAM73A as a prognostic predictor and potential therapeutic target.

Methods

Clinical samples and cell lines

Primary GC samples in this study were obtained from 100 patients who underwent radical resection for GC in the Department of Gastric Surgery, the First Affiliated Hospital of Nanjing Medical University between 2015 and 2016. No patient received adjuvant chemotherapy before surgery. This study was approved by the Ethics Committee of the First Affiliated Hospital of Nanjing Medical University and all participants provided written informed consent.

All human GC cells, including AGS, HGC27, MKN45, MGC803, SGC7901, BGC823 and normal human gastric epithelial cell line, GES-1 cell lines were purchased from Shanghai Institutes for Biological Sciences. All cell lines were cultured in RPMI-1640 (Gibco, USA) supplemented with 10% fetal bovine serum (WISENT, Canada) and antibiotics (1% penicillin/streptomycin; Gibco) and incubated in a humidified cell chamber (5% CO_2, 37 °C).

RNA extraction and quantitative real-time polymerase chain reaction

Total RNA was extracted by TRIzol reagent (Invitrogen, Carlsbad, CA, USA), the nuclear and cytoplasmic fractions were isolated by NE-PER Nuclear and Cytoplasmic Extraction Reagents (Thermo Scientific) according to the manufacturer's protocols. Concentration and quality of isolated RNA were measured by NanoDrop spectrophotometer (ND-100, Thermo). Reverse transcription of miRNA was performed using a New Poly(A) Tailing Kit (ThermoFisher Scientific, China). For circRNA and mRNA, total RNA was reverse transcribed to cDNA by PrimeScript RT Master Mix Kit (Takara, RR036A, Japan). qRT-PCR was conducted using Universal SYBR Green Master Mix (4913914001, Roche) with a 7500 Real-Time PCR System (Applied Biosystems, USA). The levels of miRNA were normalized by small nuclear U6 and *GAPDH* was used as an internal control for the relative expression of circRNA and mRNA. The relative expression levels were calculated using $2^{-\Delta\Delta CT}$ method and the primers used are listed in Supplementary Table S1.

Actinomycin D and RNase R treatment

BGC823 and SGC7901 cells were seeded at a 24-well plate overnight. Total RNA was extracted after treatment with Actinomycin D (2 mg/ml) or DMSO (Sigma-Aldrich, USA) for different periods of time (0 h, 6 h, 12 h, 18 h, 24 h). Total RNA (5 μg) was incubated with or without 20U RNase R (Geneseed, China) at 37 °C for 20 min. After treatment with Actinomycin D or RNase R, the stability of circFAM73A and FAM73A mRNA were measured by qRT-PCR.

Western Blot and immunoprecipitation

Total protein was extracted with RIPA lysis buffer. Protein concentrations were measured by BCA protein assay kit (Beyotime Biotechnology, Jiangsu, China). Cell lysis was separated on SDS-polyacrylamide gels and then transferred onto polyvinylidene difluoride (PVDF) membranes. After blocked in 5% skim powdered milk for 2 hr, the membranes were incubated with primary antibodies overnight at 4 °C and with HRP-conjugated secondary antibodies for 2 hr at room temperature. The blots were visualized by ECL chemiluminescent reagent (Millipore, MA, USA). The antibodies used in this study were listed in Supplementary Table S2.

For immunoprecipitation, GC cells were washed with 4 °C PBS followed by lysis in lysis buffer. After pre-clearing with Protein A/G PLUS-Agarose (SC-2003, SANTA CRUZ), cell lysates were immunoprecipitated with indicated antibodies. Purified immunoglobulin G (IgG) from host species was used as control. Protein A/G PLUS-Agarose was subsequently used to capture the immuno-complexes. Immunoprecipitated proteins were eluted by boiling in SDS-PAGE loading buffer and analyzed by Western Blot.

Transfection

Human circFAM73A expression vector, si-circFAM73A expression vector were purchased from Genechem (Shanghai, China). miR-490-3p mimics and inhibitors were synthesized by GenePharma (Shanghai, China). The transfection procedure was carried out with Lipofectamine 3000 (Invitrogen) in accordance with the manufacturer’s instructions. For stable transfection, respective lentivirus was constructed by Genechem (Shanghai, China) and transfected according to manufacturer’s protocols.

Cell Counting Kit-8 and colony formation assays

The Cell Counting Kit-8 (CCK-8) (Dojindo, Japan) method was performed to investigate cell proliferation. Cells were seeded into 96-well plates at a density of 1500 cells per well. The optical density (OD) values at 450 nm of each well was measured every 24 h for 5 times.

To assess cell viability, 5,000 cells were seeded into 96-well plates per well. After 24 h, cells were cultured with medium containing various cisplatin concentrations for another 48 h. Cell viability was quantified by CCK-8 kits

For colony formation assay, cells were seeded into 6-well plates at a density of 500 cells per well. After 2 weeks, the colonies were fixed in methanol for 10 min and then stained with 1% crystal violet for another 20 min at room temperature. Images were captured and cell colonies were counted and analyzed.

5-Ethynyl-20-deoxyuridine (EdU) incorporation assay

EdU assay was carried out using a Cell-Light EdU DNA Cell Proliferation Kit (RiboBio, Guangzhou, China) according to manufacturer's protocols. Briefly, cells were seeded in 96-well plates and incubated with EdU (50 μM) for 2 h. After fixed in 4% paraformaldehyde, cells were stained with Apollo Dye Solution. Hoechst 33342 was used for the staining of cell nucleus. Images were captured by an Olympus microscope (Olympus, Tokyo, Japan) for five randomly fields and the percentage of EdU-positive cells was counted.

Flow cytometry

For the cell cycle assay, cells were collected and fixed in ice-cold 75% ethanol overnight. Cells were then incubated with 500 μL propidium iodide (PI) staining solution for 30 min using Cycletest Plus DNA Reagent Kit (BD Biosciences). The cell distribution was detected by flow cytometry.

For apoptosis analysis, cells were stained with the Annexin V-FITC/Propidium Iodide (PI) Apoptosis Detection Kit (BD, Biosciences #556547) and detected by flow cytometry.

For the CD44 proportion detection, cells were resuspended in PBS containing 2% FBS and incubated with FITC-conjugated CD44 (BD Biosciences, 555478) for 20 min. After incubation, cells were washed and resuspended in 300 μl PBS and analyzed using flow cytometry. FITC Mouse IgG2b κ Isotype Control (BD Biosciences, 556655) was used as control.

Sphere formation assays

Cells were seeded at a density of 5000/well into 6-well ultra-low attachment plates (Corning, NY). 1.5 ml fresh stem cell medium was added every 2 days. Stem cell medium included DMEM/F12 medium (Invitrogen, Grand Island, NY) supplemented with EGF (20 ng/ml; Invitrogen), bFGF (10 ng/ml; Invitrogen) and 2% B27 (Invitrogen, CA, USA). 10 days after being planted, spheres with diameter > 50 μm were counted and analyzed.

Organoid culture

Sterile gastric cancer tissues obtained from patients after gastric surgery were cut into small pieces and digested with collagenase A at room temperature for 40 min. After that, cells were resuspended in Matrigel (R&D Systems, Minneapolis, MN, USA). 50 μL of Matrigel containing cells with growth factors was seeded in a 24-well plate and supplemented with 500 μl of Organoid Growth Medium (human) (Stemcell Technologies, Vancouver, Canada) for organoid growth. Photographs of human GC organoid were taken daily by microscope.

Biotinylated RNA pull-down assay

The biotin-coupled cricFAM73A probe, control oligo probe, miR-490-3p wild-type and mutated-type probe were synthesized by RiboBio (Guangzhou, China). The biotin-coupled RNA complex was pulled down by incubating streptavidin-coated magnetic beads (Invitrogen, Carlsbad, USA) with GC cell lysates according to the manufacturer's instructions. RNA bound to the beads were extracted by TRIzol (Invitrogen) and the enrichment of RNA were analyzed by qRT-PCR

Luciferase reporter assay

Luciferase reporter vector were constructed containing the wild-type sequences of circFMA73A or 3'-UTR of *HMGA2* and the mutated-type constructions were performed according to the binding sites. Luciferase reporter vectors were then co-transfected with miR-490-3p mimic or control vectors. Forty-eight hours after transfection, the relative luciferase activity was calculated as the ratio between Firefly and Renilla luciferase activities detected by a dual-luciferase system (Promega, Madison, WI).

Chromatin immunoprecipitation assay

Pierce™ Magnetic ChIP Kit (26157, Thermo Fisher Scientific) was applied for the Chromatin Immunoprecipitation (ChIP) assay. In brief, BGC823 and SGC7901 cells were fixed by adding 37% formaldehyde to a final concentration of 1% and then terminated by glycine solution. Cells were then resuspended in lysis buffer. Cell lysates were sonicated on ice to shear cross-linked DNA to length between 100 and 1000 bp for the sufficient pull-down efficiency. Cell lysates were precleared with protein A/G magnetic beads before incubating with E2F1 antibody (3742, Cell Signaling Technology) or control antibody normal rabbit IgG (12–370, Sigma-Aldrich) overnight at 4 °C. After incubation with antibodies, protein A/G magnetic beads were added to capture antibody/histone/DNA complex. Before DNA extraction, 1/5 of the cell lysate was take out for Western Blot analysis. The DNA was then extracted and the target DNA was detected by qRT-PCR. The primers designed for ChIP assay according to the potential E2F1 binding sites in FAM73A promoter region were listed in Supplementary Table S1.

RNA-binding protein immunoprecipitation assay

RNA-binding protein immunoprecipitation assay was performed by Magna RIP™ RNA-Binding Protein Immunoprecipitation Kit (17–700, Merck Millipore) according to the manufacturer's protocols. Briefly, BGC823 and SGC7901 cells in plates were cross-linked by 1% formaldehyde after washing with 4 °C PBS and then lysed in lysis buffer. Cell lysates were then sonicated on ice. HNRNPL antibody (65043, Cell Signaling Technology) or control antibody normal rabbit IgG (12–370, Sigma-Aldrich) were incubated

with washed magnetic beads for 30 minutes at room temperature. The beads-antibody complexes were then incubated with cell lysates overnight at 4 °C. The RNA was extracted and measured by qRT-PCR. The primers designed for RIP assay according to the potential HNRNPL binding sites within flanking introns of circFAM73A were listed in Supplementary Table S1.

RNA fluorescence in situ hybridization (FISH)

Fam-labeled circFAM73A and Cy3-labeled miR-490-3p probes were designed and synthesized by Servicebio (Wuhan, China). FISH experiments were performed according to the manufacturer's protocols. Briefly, for cell assay, cells were fixed in 4% paraformaldehyde and permeabilized with 0.1% Triton X-100. For GC tissues, 4-mm thick sections were cut from paraffin-embedded blocks, and then deparaffinised and rehydrated. Hybridization of cell or tissue was performed with specific probes in a dark moist chamber at 37 °C overnight. The slices were sealed with parafilm containing DAPI. Images were acquired by Leica SP5 confocal microscope system (Leica Microsystems, Mannheim, Germany).

Immunohistochemistry (IHC) staining

All specimens were fixed in 4% formalin, embedded in paraffin and sectioned into 5 mm. The 5 μm sections were incubated with primary antibodies (HMGA2, Proteintech 20795-1-AP; CD44,Abcam ab157107) overnight at 4 °C, followed by incubation with secondary antibodies at room temperature for 30 min. Next, sections were stained with DAB solution for 5 minutes. The IHC staining were scored by the percentage of positive cells (graded as 0, < 5%; 1, 5%-25%; 2, 26%-50%; 3, 51%-75%; and 4, > 75%) and the intensity of cell staining (graded as 0, no staining; 1, weak; 2, moderate; and 3, strong).

Animal experiment

Four -week-old female BALB/c nude mice were purchased from the Department of Laboratory Animal Center of Nanjing Medical University. All the animal studies were approved by Nanjing Medical University Ethics Committee.

For xenografts tumors growth assay, 1×10^6 transfected cells suspended in 100 μL were subcutaneously injected into the axilla of nude mice. The width and length of the tumors were measured once a week and the tumor volumes were calculated as $(\text{width}^2 \times \text{length})/2$. Four weeks after injection, the mice were sacrificed and tumor weights were measured.

For lung metastasis model, transfected luciferase-labeled cells were injected into the caudal veins of mice and metastasis were monitored using an in vivo imaging systems (IVIS). 6 weeks after injection, mice were sacrificed and lung tissues were harvested for hematoxylin-eosin staining.

For liver metastasis model, cells were injected into the portal veins of mice and 6 weeks after injection, mice were sacrificed and liver tissues were harvested for hematoxylin-eosin staining.

Statistical analysis

Statistical analyses were conducted by SPSS 20.0 (IBM, SPSS, IL, USA) and GraphPad Prism. And all data were presented as mean ± standard deviation (S.D.). Student's t-test was performed to assess statistical significance between two groups. The Pearson's correlation analysis was used to analyze the association between circFAM73A expression with clinicopathologic parameter. Overall survival (OS) was analyzed by the Kaplane-Meier method and log-rank test. Univariate analysis and multivariate models were performed with Cox proportional hazards regression models.

Results

CircFAM73A is upregulated in GC and high circFAM73A predicts poor prognosis

To assess the circRNA involved in GC, we searched the circRNA datasets established for gastric cancer in the GEO DataSets. Six datasets were found, and GSE83521, was chosen for the subsequent analysis, as it contains the highest number of samples. Several differentially expressed circRNAs were calculated and then filtered according to their log Fold Change ≥ 2 and adjusted P value ≤ 0.01. Four circRNAs, hsa_circ_0001789, hsa_circ_0007376, hsa_circ_0052001 and hsa_circ_0002570 were screened out. Next, we verified their expression by qRT-PCR analysis in our 60 paired cancer tissues and their matched adjacent non-cancer tissues from GC patients. As shown in Fig. 1A, the most significant expression change was observed for hsa_circ_0002570, thus prompting us to further investigate its role in GC malignancy.

Hsa_circ_0002570 (circFAM73A) originates from exon 3,4,5,6,7 of the FAM73A genome (UCSC data in NCBI) (Fig. 1B). We validated the head-to-tail back splicing in RT–PCR product of circFAM73A using Sanger sequencing (Fig. 1C). qRT-PCR results showed the highest circFAM73A abundance in BGC823 cells and the lowest in SGC7901 cells (Fig. 1D). We therefore selected BGC823 and SGC7901 cell lines for subsequent studies. As shown in Fig. 1E, circFAM73A was resistant to the digestion of RNase R exonuclease compared to the linear form of FAM73A in BGC823 and SGC7901. In order to avoid the possibilities of trans-splicing or genomic rearrangements, we conducted several universal circRNA detection experiment[23]. We first designed divergent primers to amplify circFAM73A and convergent primers to amplify FAM73A mRNA. Using cDNA (complementary DNA) and gDNA (genomic DNA) from BGC823 and SGC7901 and two randomly GC tissues as templates, circFAM73A was only amplified from cDNA by divergent primers, whereas no amplification product was obtained when using gDNA (Fig. 1F). Actinomycin D, an inhibitor of transcription, was then used to measure the half-life of circFAM73A and FAM73A in BGC823 and SGC7901. The results indicated that circFAM73A was more stable than FAM73A mRNA (Fig. 1G and Figure S1A). These findings clearly showed that the circular characteristics of circFAM73A.

Next, we examined the relative expression levels of circFAM73A in the cytoplasm and nuclear compartments of BGC823 and SGC7901. qRT-PCR demonstrated that circFAM73A preferentially localized

in the cytoplasm (Fig. 1H and Figure S1B), which was confirmed using fluorescence in situ hybridization (FISH) against circFAM73A (Fig. 1I and Figure S1C).

High expression of circFAM73A was then authenticated in an additional 100 paired GC tissue samples (Fig. 1J) using qRT-PCR. 63% samples (n = 63) exhibited higher expression levels in the cancer tissue samples than in matched noncancerous tissue samples (Figure S1D and S1E). Our analysis of clinicopathological characteristics showed that circFAM73A expression significantly correlates with TMN stage and tumor size (Table 1). The expression of circFAM73A in tumor tissues at III stage was notably higher than that at I-II stage and in matched adjacent tissues, whereas abundance in tumors at I-II stage showed no difference from that in noncancerous tissues (Fig. 1L). Similarly, we also found that the expression in tumors larger than 3 cm was considerably higher than that in tumors smaller than 3 cm and in adjacent tissues (Fig. 1M). In contrast, other clinicopathological characteristics including age, gender, tumor site, lymph node metastasis or blood vessel invasion (Figure S1F-1J) showed no correlation. Moreover, GC patients with higher circFAM73A expression had significantly shorter overall survival than those with the lower circFAM73A expression by Kaplan–Meier survival analysis (Fig. 1K). Further Cox multivariate survival analysis revealed high circFAM73A expression as an independent prognostic factor for poor survival of GC patients (hazard ratio [HR] = 2.171, 95% confidence interval [CI] = 1.015–4.645, p = 0.046) (Table 2). In contrast, no obvious change of linear FAM73A mRNA was found in our GC samples (Figure S1K), and FAM73A showed no correlation with the prognosis of GC patients both in our samples and TCGA database (Figure S1L and S1M).

Table 1
Correlation between circFAM73A expression and the clinicopathologic parameter of 100 GC patients. * $p < 0.05$, ** $p < 0.01$.

Clinicopathologic parameter		Number	Number of patients		*p* value
			circFAM73A^{low}	circFAM73A^{high}	
Age	< 60 years	36	16	20	0.532
	≥ 60 years	64	34	30	
Gender	Male	75	39	36	0.645
	Female	25	11	14	
Tumor size	< 3 cm	26	19	7	0.011*
	≥ 3 cm	74	31	43	
Tumor site	Proximal	44	24	20	0.546
	Non-proximal	56	26	30	
Lymph node metastasis	N0	38	24	14	0.063
	N1-N3	62	26	36	
TMN stage	I-II	44	28	16	0.026*
	III	56	22	34	
Blood vessel invasion	Negative	73	40	33	0.176
	Positive	27	10	17	

Table 2
Univariate and Multivariate Cox regression analysis of overall survival in 100 GC patients, * $p < 0.05$, ** $p < 0.01$, *** $p < 0.001$.

Clinicopathologic parameter	Overall Survival			
	Univariate analysis		Multivariate analysis	
	HR (95% CI)	p value	HR (95% CI)	p value
Age (≥ 60 years vs < 60 years)	0.850 (0.412–1.751)	0.659		
Gender (Female vs Male)	1.659 (0.781–3.524)	0.188		
Tumor size (≥ 3 cm vs < 3 cm)	1.292 (0.557–2.999)	0.551		
Tumor site (Proximal vs Non-proximal)	1.284 (0.623–2.646)	0.497		
Lymph node metastasis (N1-N3 vs N0)	3.196 (1.310–7.799)	0.011*	2.806 (1.140–6.902)	0.025*
TMN stage (III vs I-II)	2.860 (1.278–6.402)	0.011*		
Blood vessel invasion (Positive vs Negative)	2.004 (0.972–4.132)	0.060		
circFAM73A expression (High vs Low)	2.518 (1.185–5.349)	0.016*	2.171 (1.015–4.645)	0.046*

Taken together, these data proved the upregulation of circFAM73A in GC and its clinical significance in GC patients.

CircFAM73A promotes the proliferation, migration and facilitates cisplatin resistance of GC in vitro

To disentangle the biological function of circFAM73A, two siRNAs were designed to specifically target the back-splice junction (Figure S2A). Si-circ-1 successfully suppressed circFAM73A expression with no effects on the levels of linear FAM73A in BGC823 and SGC7901 (Figure S2B). In addition, we also transfected overexpression vectors into both cell lines and the efficiency was verified via qRT-PCR (Figure S2C).

We first performed colony formation and CCK8 assay to examine the effects of circFAM73A on cell proliferation. The results showed that transfecting with siRNA dramatically suppressed the proliferation of BGC823 and SGC7901. In contrast, exogenous expression of circFAM73A exerted the opposite effects (Fig. 2A and 2B). Next, 5-ethynyl-2'-deoxyuridine (EdU) incorporation assay also demonstrated that circFAM73A increased the rate of EdU incorporating cells (Fig. 2C and Figure S2D). A 3D GC organoid

model was then established to further test the proliferation ability. We found that silencing of circFAM73A significantly decreased the diameter of organoids and the opposite findings were acquired in circFAM73A reconstitution groups (Fig. 2D and Figure S2E). To analyze whether circFAM73A interfered with cell cycle, we then measured cell-cycle distribution using flow cytometry. As shown in Fig. 2E, interference of circFAM73A expression distinctly increased the percentage of G0/G1 phase cells and diminished the S phase cells, while over-expressing circFAM73A showed the opposite trend. These observations indicated that interference of circFAM73A induced cell-cycle arrest in the G0/G1 phase, thereby constrained the proliferation of GC cells. Moreover, cell migration was impeded by circFAM73A depletion and fortified by overexpressing circFAM73A in both BGC823 and SGC7901 based on Transwell assay (Fig. 2F).

For advanced or metastatic GC patients, chemotherapy based on cis-dichlorodiammine platinum (CDDP) /cisplatin is currently recommended as first-line therapy. We therefore assessed the effects of circFAM73A on the chemo-sensitivity of GC cells. BGC823 and SGC7901 cells resistant to CDDP (referred to as BGC823CDDP and SGC7901CDDP cells) were established as described before[24]. As shown in Figure S3A, circFAM73A expression was considerably increased in BGC823CDDP and SGC7901CDDP cells compared with the corresponding sensitive cells by qRT-PCR. To test whether circFAM73A modulated the sensitivity of cisplatin treatment in GC cells, we treated cells with various concentrations of CDDP. circFAM73A over-expression reinforced cell viability and elevated the IC50 in BGC823 and SGC7901 cells (Figures S3B and S3C), whereas reduction of circFAM73A in BGC823CDDP and SGC7901CDDP cells showed the reverse effects (Figures S3D and S3E). Our colony formation assay demonstrated that up-regulation circFAM73A enhanced the long-term viability of CDDP-sensitive cells. In comparison, down-regulation circFAM73A displayed the opposite results in CDDP- resistant cells (Figures S3F). Moreover, results of flow cytometry assay exhibited that circFAM73A reduced the apoptosis rates of GC cells treated with CDDP (Figures S3G).

Collectively, these findings demonstrated that circFAM73A promotes GC cell proliferation, migration and facilitates cisplatin resistance of *in vitro*.

CircFAM73A enhances the stem cell-like property in GC cells

A growing number of studies suggest that the acquisition of cancer stem cell-like properties is crucial for the initiation and maintenance of the malignancy process of GC[3, 4]. Given the facilitating role of circFAM73A on cell proliferation and cisplatin resistance, we asked whether circFAM73A enhances the stem cell-like properties of GC cells.

We first explored the role of circFAM73A on the ability of GC cells self-renew. To this end, we performed a sphere formation assay. As shown in Fig. 3A and 3B, Overexpression of circFAM73A promoted the generation and cell content of tumor spheres of BGC823 and SGC7901 cultured in suspension. Conversely, circFAM73A-silenced cells formed fewer spheres with lower cell content. The induction of circFAM73A in the self-renewal ability was also confirmed using limiting dilution assay (Fig. 3C).

In addition, augmentation of circFAM73A increased, while downregulation of circFAM73A reduced the proportion of CD44 (GC stem cell-like marker) positive cells in BGC823 and SGC7901 (Fig. 3D). By qRT-PCR and Western blot showed that circFAM73A significantly increase expression of CD44 and the stemness-associated transcriptional factors including SOX-2, OCT-4 and Nanog. The opposite results were acquired in circFAM73A-depressed cells (Fig. 3E and 3F).

Together, these findings supported that circFAM73A exhibits a positive effect on CSC-like properties in GC cells.

CircFAM73A acts as a sponge of miR-490-3p, HMGA2 is the direct downstream target of miR-490-3p

CircRNAs function primarily as miRNA sponges by sequestering specific miRNAs, resulting in the changes of specific genes expression. We therefore investigated the potential miRNAs associated with circFAM73A.

In consideration of the elevated expression and the promotive effects of circFAM73A in GC, we screened the predicted miRNA targets obtained from TargetScan and RNAhybrid together with miRNAs that were significantly downregulated in GC samples according to TCGA database (fold change > 2, $p < 0.05$) (Fig. 4A). We identified 8 candidate miRNAs that matched these criteria (Figure S4A). A biotin-labeled circFAM73A probe was then designed to examine the potentially miRNAs that interacted with circFAM73A. The probe efficiency was verified in GC cells while circFAM73A overexpression further enhanced the pull-down efficiency (Figure S4B). As shown in Fig. 4B, qRT-PCR revealed that miR-490-3p was the only one that was pulled down by circFAM73A probe in both BGC823 and SGC7901. To further verify the direct binding of circFAM73A and miR-490-3p, luciferase reporter assays were then carried out, which demonstrated that overexpression of miR-490-3p considerably decreased the luciferase activity of the reporter containing the wild type circFAM73A sequence, but had no effects on the reporter containing circFAM73A with mutant miR-490-3p-binding site in BGC823 and SGC7901 (Fig. 4C). Furthermore, in comparison with the mutant biotin-labeled miR-490-3p, wild-type miR-490-3p captured more circFAM73A in GC cells with circFAM73A overexpression (Fig. 4D). FISH assay showed the co-location in cytoplasm between circFAM73A and miR-490-3p (Fig. 4E). The reduction of miR-490-3p in GC tissues was also found in our samples (Figure S4C). These results suggested that circFAM73A exerts its function by sponging miR-490-3p.

To identify miR-490-3p target genes, we screened TCGA for genes that were significantly upregulated in GC (fold change > 2, $P < 0.05$), combined with the predicted targets from TargetScan (Fig. 4F). Using this strategy, we identified 14 genes. We then analyzed the correlations between miR-490-3p expression and these 14 candidate targets in TCGA GC database. Four genes (AURKA, ONECUT2, RNF207 and HMGA2) showed clear negative correlation with miR-490-3p (Fig. 4G and Figure S4D), and were therefore chosen for further experiments.

qRT-PCR verified the upregulation of AURKA, ONECUT2 and HMGA2 in our 100 paired GC tissues compared with adjacent tissues, whereas no significant changes in RNF207 expression were observed (Fig. 4H). Moreover, ONECUT2 and HMGA2 expression levels exhibited a clear negative correlation with miR-490-3p, while we found no such correlation for AURKA and RNF207 (Fig. 4I). As shown in Fig. 4J and S4E, overexpression of miR-490-3p reduced the expression of ONECUT2 and HMGA2, in comparison, inhibition of miR-490-3p increased the expression of ONECUT2 and HMGA2. However, expression of AURKA and RNF207 showed no change after miR-490-3p overexpression or inhibition. Next, siRNAs specific to these four genes were transfected into GC cells. Only interference sequence of AURKA and HMGA2 suppressed the viability by CCK-8 assay in BGC823 and SGC7901 cells (Figure S4F and S4G).

On the basis of these results, we chose HMGA2, a potential tumor promotor and target of miR-490-3p in GC, for further studies. Luciferase reporter assays confirmed that HMGA2 was a direct downstream target of miR-490-3p (Figure S4H and S4I). Importantly, Kaplan–Meier survival analysis in our 100 GC patients and TCGA database showed that higher HMGA2 expression correlates with poor overall survival in GC patients (Fig. 4K and 4L).

CircFAM73A regulates HMGA2 expression by miR-490-3p

High Mobility Group A2 (HMGA2) is a stem cell factor primarily expressed during embryogenesis, with low abundance identified in adult human tissues[25]. HMGA2 is aberrantly expressed in several types of cancer, with high levels of HMGA2 associated with a highly malignant phenotype, as it relates with increased tumor proliferation, invasiveness, stemness and reduced survival[26–28]. As shown in Fig. 5A, a positive correlation between mRNA levels of circFAM73A and HMGA2 was detected in GC tissues, implying the potential regulation of circFAM73A on HMGA2 in GC.

To assess whether circFAM73A regulates HMGA2 expression by miR-490-3p, we reduced miR-490-3p expression in circFAM73A-repressing cells and elevated miR-490-3p in circFAM73A-overexpressing cells. Our Western Blot and qRT-PCR data showed that circFAM73A increased the expression of HMGA2 while the miR-490-3p mimic attenuated this effect. In contrast, reduction of HMGA2 caused by circFAM73A inhibition also reversed by miR-490-3p knocking-down both in BGC823 and SGC7901 (Fig. 5B, Figure S5A and S5B). Moreover, flow cytometry demonstrated that circFAM73A exogenous expression increased the proportion of CD44 positive cell and this effect was reversed by miR-490-3p mimic. In comparison, circFAM73A suppression led to the decline of CD44 positive cells which was also overturned by miR-490-3p inhibition (Fig. 5C and Figure S5C). The same results were also acquired when we examined the effects of circFAM73A on other stemness-associated transcriptional factors (SOX-2, OCT-4 and Nanog) by Western Blot (Fig. 5D and Figure S5D).

In addition, FISH assay showed the co-localization between circFAM73A and miR-490-3p in GC tissues. FISH scores confirmed that expression of circFAM73A was higher in GC tissues than in matched noncancerous tissues, whereas miR-490-3p expression showed the adverse change (Fig. 5E). Similarly, IHC staining also exhibited the increase of HMGA2 protein levels in GC tissues (Fig. 5F and5G).

Importantly, we found that circFAM73A, miR-490-3p and HMGA2 correlated well in these GC tissues (Fig. 5H).

These observations supported that circFAM73A regulates the HMGA2 expression and stemness-related pathway by sponging miR-490-3p.

CircFAM73A promotes stem cell-like property and cell malignancy in GC cells by upregulating HMGA2 expression

Based on the results above, we hypothesized that circFAM73A improves stem cell-like property and cell malignancy in GC by sponging miR-490-3p, thus upregulating HMGA2 expression. To test this hypothesis, we either repressed or reconstituted HMGA2 expression in circFAM73A overexpressed or silenced cells, respectively.

Using a sphere formation assay, we found that the induction of circFAM73A on cell self-renewal ability was counteracted by HMGA2 downregulation. While HMGA2 reconstitution reversed the inhibitory function of circFAM73A repression (Fig. 6A and Figure S6A). Similarly, HMGA2 downregulation also impaired the capability on cell proliferation and migration caused by exogenous circFAM73A expression and ectopic HMGA2 expression overturn the inhibitory effects of circFAM73A suppression based on the results of further experiments including colony formation assay (Fig. 6B and Figure S6B), EdU assay (Fig. 6C and Figure S6C), flow cytometry (Fig. 6D and Figure S6D) and Transwell assay (Fig. 6E and Figure S6E).

Together, these results confirmed that circFAM73A promotes the cancer stem cell-like properties and cell malignancy in GC cells by upregulating HMGA2 expression.

CircFAM73A regulates HMGA2 expression level to promote GC growth and metastasis in vivo

To delineate the roles of circFAM73A and HMGA2 *in vivo*, we first generated xenografts tumors in nude mice. Xenograft tumors generated from circFAM73A-overexpressing BGC823 cells showed considerably faster growth, whereas circFAM73A-suppressed xenografts were smaller in volume than those formed from control cells. Moreover, repressing HMGA2 expression reversed the positive effect of circFAM73A on xenograft tumors formation, while exogenous expression of HMGA2 attenuated the effects caused by cirFAM73A disruption (Fig. 7A-7C, Figure S7A and S7B). Our qRT-PCR results showed that circFAM73A increased the mRNA levels of HMGA2 and CD44 in xenograft tumors samples, an effect that was reversed by HMGA2 depletion (Figure S7C). In contrast, exogenous HMGA2 expression reversed the reduction caused by cirFAM73A suppressing (Figure S7D). Immunohistochemistry staining of HMGA2 and CD44 in xenograft tumors demonstrated the same effects (Fig. 7G and 7H).

To examine the metastasis abilities of circFAM73A and HMGA2, we established two *in vivo* models. In lung metastasis model, respective tumor cells were injected into the caudal veins of mice and metastasis were monitored by an IVIS Imaging system. After 6 weeks, mice were euthanized. The lung tissues were obtained for HE staining (Fig. 7D) and lung metastatic foci were quantified (Fig. 7E and 7F). In liver

metastasis model, tumor cells were injected into the portal veins of mice. Livers were harvested after 6 weeks and stained with HE (Fig. 7I). The number of nodes were counted (Figure S7E and S7F) and the liver indexes (liver weight/ body weight) were calculated (Fig. 7J). These two models clearly showed that circFMA73A enhanced the metastasis of GC *in vivo*, which was also mediated by HMGA2

Together, these data confirmed that circFAM73A promotes both GC growth and metastasis *in vivo* via regulating HMGA2 expression levels.

HMGA2 enhances the transcriptional activation of FAM73A by E2F1 and elevates the efficiency of cirFAM73A circularization by HNRNPL, which in turn elevates circFAM73A expression

HMGA2 functions as an architectural transcription modulator and facilitate the function of several transcription factors, including E2F1. Previous studies revealed that the interaction between HMGA2 and pRB enhances the activation of E2F1 in pituitary adenomas[26]. We then investigated whether HMGA2 facilitate the function of E2F1 in GC.

Firstly, the immunoprecipitation assay confirmed the interactions between HMGA2 and pRB in GC cells (Fig. 8A). We then examined the effects of HMGA2 on E2F1 activity by measuring the expression of several classical E2F1 responsive effectors (CDC2, CCNE1 and TK1). Western blot and qRT-PCR demonstrated that both protein and mRNA levels of these effectors increased by ectopic expression of HMGA2 and declined by HMGA2 repressing (Fig. 8B, Figure S8A and S8B). However, no change of E2F1 expression was detected upon HMGA2 alteration, suggesting that HMGA2 might simply increase the activity of E2F1, rather than its expression in GC.

Intriguingly, two putative binding sites of E2F1 were found in the FAM73A promoter region using JASPAR (#1 ATGGCGGGAGC, -77 to -67, #2 GGCCCGCCAAA, -696 to -686) (Fig. 8C). We therefore investigated whether E2F1 promotes the transcription of FAM73A and results in the increase of FAM73A mRNA or circFAM73A. qRT-PCR by specific primers (Figure S8C) showed that pre-FAM73A, FAM73A and circFAM73A levels were increased following E2F1 overexpression, while being suppressed upon E2F1 depletion (Fig. 8D and Figure S8D). To examined the binding of E2F1 on FAM73A promoter, luciferase reporter gene assay was performed. As shown in Fig. 8E and Figure S8E, E2F1, rather than vector plasmid, elevated the luminescence of the luciferase reporter containing FAM73A promoter region. ChIP-PCR analysis using specific antibody against E2F1 confirmed the occupancy of E2F1 on binding site #1 in FAM73A promoter region. Moreover, this effect could be promoted by HMGA2 ectopic expression (Fig. 8F and 8G, Figure S8F and S8G), indicating that HMGA2 enhanced the transcription of FAM73A by E2F1. As expected, HMGA2 increased both pre-FAM73A and circFAM73A production. However, elevated pre-FAM73A caused by HMGA2 induction only resulted in the increase of circFAM73A, but not linear FAM73A mRNA (Fig. 8H and Figure S8H).

The uncorrelated levels of circular RNAs and linear mRNAs indicated that HMGA2 might also affect the post-transcriptional processing and increase the back-splicing efficiency in pre-FAM73A, making circular RNAs the preferred gene output than linear RNAs. Mounting evidence suggests that splicing factors

contribute to circRNA biogenesis post-transcriptionally by targeting specific sequence within flanking introns and drawing back-splicing exons ends into close proximity[20, 29, 30]. We then utilized the MEME Suite[31] to analyze the known RBPs binding motifs in flanking intron-2 and intron-7 of circFAM73A ($p < 0.001$, $q < 0.5$). Several RBPs motifs were found and among them, HNRNPL was predicted to harbor binding sites on both intron-2 and intron-7 (Figure S8I) and was previously confirmed to promote circRNA circularization[32].

To identify the direct HNRNPL binding sites in the flanking intron of circFAM73A, we performed RNA-immunoprecipitation (RIP) assays, using qRT-PCR to quantify HNRNPL occupancy within the introns adjacent to circFAM73A-forming exons. Three pairs of primers were designed according to the potential binding sequences. Primer 1 contains the three predicted HNRNPL binding sites in intron-2. Primer 2 targets the first predicted binding sites in intron-7 and the 2 to 6 predicted binding sites in intron-7 are covered in the amplification sequence of Primer 3 (Fig. 8I). We found that HNRNPL bound to Primer 1 region in intron-2 and Primer 3 region in intron-7, rather than Primer 2 region (Fig. 8J and Figure S8J). Furthermore, knock down of HNRNPL resulted in a significant reduction of circFAM73A but not pre-FAM73A. In addition, we also observed a small but significant increase of FAM73A mRNA (Fig. 8K and Figure S8K). Together, these findings demonstrated that HNRNPL binds to the flanking intron region and elevates the circFAM73A formation.

We then investigated whether HMGA2 promotes the circularization of circFAM73A by HNRNPL. The ratio of circRNA expression to mRNA expression was calculated to reflect the circularization efficiency. As shown in Fig. 8L and Figure S8L, exogenous HMGA2 expression resulted in the upregulation of circularization efficiencies, which was reduced when HNRNPL was additionally suppressed, suggesting that HMGA2 enhances the efficiency of cirFAM73A circularization by HNRNPL.

In addition, we also found that both E2F1 and HNRNPL correlated well with HMGA2 in TCGA database (Fig. 8M and 8N), which indicated the regulation of E2F1 and HNRNPL on circFAM73A and its downstream target, HMGA2.

Collectively, these results demonstrated that HMGA2 plays a dichotomous role on regulating circFAM73A expression, i.e. HMGA2 facilitates the transcriptional activation of FAM73A by E2F1 and elevated the efficiency of cirFAM73A circularization by HNRNPL.

CircFAM73A directly interacts with HNRNPK and facilitates β-catenin stabilization

To further explore the mechanism of circFAM73A, an RNA pulldown assay was conducted using a specific biotin-labeled circFAM73A probe. Coomassie blue staining showed several bands of proteins compared with antisense probe (Fig. 9A) while mass spectrometry analysis identified HNRNPK (Fig. 9B), one of the major pre-mRNA-binding proteins. The RIP assay confirmed the direct interaction between circFAM73A and HNRNPK (Fig. 9C and Figure S9A). However, the expression of HNRNPK showed no obviously change upon circFAM73A overexpression or knocking-down by Western Blot (Fig. 9D and

Figure S9B) in BGC823 and SGC7901, indicating that circFAM73A might regulate the activity rather than the expression of HNRNPK.

It has been reported that several lncRNA interacts with HNRNPK and facilitates the HNRNPK-mediated stability of β-catenin. Co-IP analysis was performed and indicated the endogenous interaction between HNRNPK and β-catenin in GC cells (Fig. 9E and Figure S9C). We therefore investigated whether circFAM73A regulates the expression of β-catenin by HNRNPK. Western Blot demonstrated that ectopic expression or knockdown of circFAM73A increased or decreased β-catenin levels (Fig. 9F and Figure S9D). Moreover, the reduction of β-catenin caused by circFAM73A repression was abolished by MG132 treatment (Fig. 9G and Figure S9E). Besides, after treatment of cycloheximide, Western Blot assay showed that circFAM73A knocking-down shortens the half-life of β-catenin (Fig. 9H and Figure S9F), indicating that circFAM73A stabilizes β-catenin by reducing the degradation of β-catenin protein. We then investigated the roles of circFAM73A in HNRNPK-mediated β-catenin stability, and found that ectopic expression or knockdown of circFAM73A promoted and weakened the interaction between HNRNPK and β-catenin in GC cells (Fig. 9I and Figure S9G), respectively. Moreover, overexpression or knockdown of circFAM73A also resulted in increase and decrease of nuclear translocation and of β-catenin (Fig. 9J and Figure S9H).

Furthermore, functional experiment showed that the promoting effects of circFMA73A were reversed upon HNRNPK interfering (Fig. 9K-9M and Figure S9I-S9K), demonstrating HNRNPK as the downstream of circFAM73A.

Taken together, our results indicated that circFAM73A directly interacts with HNRNPK and facilitates the stabilization of β-catenin.

Discussion

Despite the clinical application and continuous progress of systemic treatments in gastric cancer, gastric cancer remains to be a high-mortality malignancy[1]. Cancer stem cells (CSCs) represent the composition that holds the capacities of self-renewal and differentiation in cancer cells[2] and to some extent, the proposal of CSCs model explicated the high postoperative relapse and the resistance of cancer under current systemic treatments[33].Therefore, deep understanding of the biology and regulatory mechanism of CSCs holds enormous potential for developing new classes of therapeutics in cancer. However, studies concentrated on the effects of circRNAs on cancer stem cell-like properties are still comparatively insufficient.

Here, by screening GEO datasets and verifying in our samples, we identified a circRNA originated from 3,4,5,6,7 exons of FAM73A (circFAM73A) whose expression is relatively upregulated in GC and then focused our investigates on the role and potential mechanism of circFAM73A in GC malignancy. Further Cox multivariate survival analysis revealed high circFAM73A expression as an independent prognostic factor for poor survival of GC patients, which implied its tumor-prompting effects. Further functional

experiment demonstrated that circFAM73A reinforced the stem cell-like property in GC, thus, exerting the facilitating role on cell proliferation, migration and cisplatin resistance.

The specific mechanisms of circRNA function in cancer progression have not been entirely elucidated[34]. The most widely studies of circRNAs regard it as the competing endogenous RNA. This hypothesis supposes that circRNAs could serve as decoys of available miRNAs, functionally releasing those downstreams targeted by that set of miRNAs[35]. In current study, we screened the predicted miRNA obtained from TargetScan and RNAhybrid and combined with the downregulated miRNAs in TCGA. 8 candidate miRNAs were selected and miR-490-3p was further confirmed that is capable of binding to circFAM73A by subsequently experiments. Next, for miR-490-3p target genes, we screened TCGA for upregulated genes together with predicted targets from TargetScan. Followed by bioinformatic analysis and experimental verification, HMGA2 was certified as the downstream of circFAM73A/miR-490-3p.

HMG (High Mobility Group) proteins were initially discovered in embryonic stem cells as the most abundant small, chromatin-associated DNA-binding protein[36]. However, HMGA2 expression becomes more restricted as fetal development, partly due to increasing let-7b expression[37] and is particularly low within normal mature tissues, with one exception that it is strongly expressed during spermatogenesis in testis in mice[38]. Intriguingly, independent studies have evidenced that HMGA2 is re-expressed during oncogenesis in a variety of human malignancies [26, 27], including gastric cancer, where high expression of HMGA2 correlates with lymph node metastasis, increased TNM stage and reduced patient survival in GC patients[28, 39, 40]. The aberrant expression of HMGA2 was regulated by diverse mechanism, including chromosomal rearrangements[41] or several noncoding RNA[25]. A recent study also demonstrated that N6-methyladenosine modification of circNSUN2 stabilized HMGA2 mRNA by IGF2BP2 and promoted aggressiveness of CRC cell[42]. In our study, the high level of HMGA2 in GC was observed in both TCGA dataset and our own samples, more importantly, poorer survival of high HMGA2 GC patients was also validated. These data suggested the vital role of HMGA2 in GC which was then confirmed by subsequent functional experiment both *in vitro* and *in vivo*. Here, we also expanded a novel pattern of HMGA2 regulation in which HMGA2 is verified as a direct downstream target of miR-490-3p in GC while circFAM73A functions as the sponge of miR-490-3p, thus modulates HMGA2 expression. We also proved that the facilitating effects of circFAM73A on GC is, at least partially, mediates by HMGA2.

Biogenesis of circRNAs is intricately involved by multiple factors. Generally speaking, the endogenous level of circRNAs in cells is regulated at three levels, including the transcription of circRNA-producing pre-mRNA, co- or post-transcriptional processing affecting the efficiency of back-splicing and circRNA turnovers. It was reported that transcriptional factors could modulate biogenesis of circRNAs. circHIPK3 was enriched in diabetes mellitus and colorectal cancer by c-Myb[43, 44]. Twist1 could bind Cul2 promoter and activate its transcription, resulting in the selectively upregulation of of Cul2 circular RNA, but not mRNA[45]. In our work, we demonstrated that HMGA2 interacts with pRB and enhances the activity of E2F1, which was consistent with previous study[26]. E2F1 is a well-known transcription factor with frequently hyperactivation in human malignancy and prompts transcription of a number of genes contributes to cancerous progression[26, 46, 47]. More intriguingly, we validated that E2F1 could bind the

FAM73A promoter and activate its transcription, thus elevate expression of pre-FAM73A, as well as circFAM73A. Therefore, HMGA2 regulated circFAM73A expression by E2F1 activation.

However, elevated pre-FAM73A caused by HMGA2 induction only resulted in the increase of circFAM73A, but not linear FAM73A mRNA. The uncorrelated levels of circular RNA and linear mRNA promoted us to investigated the possible involvement of HMGA2 in the formation efficiency of pre-FAM73A. Existing studies have established that binding of *trans* factor in flanking introns could elevate circRNA formation by drawing back-splicing exons ends into close proximity[30, 32]. The processing of circRNAs could modify alternative splicing of such pre-mRNAs, therefore, shifting the output of protein-coding genes to circular RNAs[29, 48]. Even if these effects might be limited, as circular RNAs are naturally resistant to exonucleases, slight alteration on efficiency of back-splicing might result in profound variations in steady-state levels of these transcripts. HNRNPL was previously confirmed to promote circRNA formation in prostate cancer[32] and the binding of HNRNPL within the flanking introns of circFAM73A was also verified via motifs scanning and RIP assay, strongly indicating its role on circFAM73A formation. It is worth to mention that knocking-down of HNRNPL not only resulted in the reduction of circFAM73A, but also caused a slight increase of FAM73A. A recent study also reported that interfering with SMN circRNAs biogenesis leads to the significant rescue of SMN protein[49], implicating the competition between canonical splicing and back-splicing, when back-splicing of exons for circRNA formation is considered as an unusual type of alternative splicing. This competition might explain the increase of linear FAM73A mRNA caused by HNRNPL depletion as it impedes the back-splicing of pre-FAM73A. Subsequent investigations verified that HMGA2 increased back-splicing efficiency in pre-FAM73A by HNRNPL. Nevertheless, further investigations are needed to understand the precise mechanism of HMGA2 regulation on HNRNPL.

These observations above suggested that HMGA2 could in turn elevated circFAM73A expression via enhancing the transcription of FAM73A by E2F1 and increasing the efficiency of circFAM73A circularization by HNRNPL, which may partially account for the positive correlation between HMGA2 and circFAM73A. These findings uncover a novel feedback loop in circRNAs regulation reciprocally that prompts GC development.

Besides acting as the sponge of miRNAs, circRNAs can also interact with different proteins that subsequently influence the function of associated proteins. To fully explore the mechanisms under circFAM73A, an RNA pulldown followed with mass spectrometry analysis was conducted to assess the potential associated proteins. HNRNPK, one of the major pre-mRNA-binding proteins, was screened out and verified. hnRNP family is known to regulate gene expression through RNA-binding domain and is involved in multiple physiological and pathological processes, such as organogenesis, erythroid differentiation, and carcinogenesis[50, 51]. Increasing evidences suggest that HNRNPK is a key interactor of ncRNAs associating in varieties aspects of human health and disease[52, 53]. Here, we demonstrated that circFAM73A binds to HNRNPK, enhances the interaction between HNRNPK and β-catenin and facilitates the stability of β-catenin, thus promotes the CSC- like properties in gastric cancer.

Conclusions

In conclusions, our work underscores a novel pathway of circFAM73A that functions on the facilitating effects on cancer stem cell-like properties in gastric cancer. More importantly, the upregulation of circFAM73A is closely correlated with the poor prognosis of GC patients. circFAM73A regulates HMGA2 expression by absorbing miR-490-3p in a positive feedback loop. circFAM73A also interacts with HNRNPK and facilitates β-catenin stabilization. These lead to the progression of gastric cancer and may provide a new insight for circRNA-based diagnostic and therapeutic strategies.

Abbreviations

CSC
Cancer stem cells; circRNA:Circular RNA; GC:Gastric cancer; FISH:Fluorescence in situ hybridization; HMGA2:High Mobility Group A2; IHC:Immunohistochemistry; Pre-mRNA:precursor mRNA; qRT-PCR:Quantitative real-time polymerase chain reaction.

Declarations

Ethics approval and consent to participate

The primary GC samples in this study were obtained from patients who underwent radical resection for GC in the Department of Gastric Surgery, the First Affiliated Hospital of Nanjing Medical University between 2015 and 2016. This study was approved by the Ethics Committee of the First Affiliated Hospital of Nanjing Medical University and all participants provided written informed consent. All the animal studies were approved by Nanjing Medical University Ethics Committee.

Consent for publication

Not applicable.

Availability of data and materials

All data in this current study are available from the corresponding author upon reasonable request.

Competing interests

The authors declare that they have no competing interests.

Funding

This work was partially supported by the National Natural Science Foundation of China (82072708, 81871946, 81602080, 81902461); Postgraduate Research & Practice Innovation Program of Jiangsu Province (SJCX20_0479); the Primary Research & Development Plan of Jiangsu Province (BE2016786); the Program for Development of Innovative Research Team in the First Affiliated Hospital of NJMU; the

Priority Academic Program Development of Jiangsu Higher Education Institutions (PAPD, JX10231801); Jiangsu Key Medical Discipline (General Surgery) (ZDXKA2016005); Six Talent Peaks of Jiangsu Province(2018 WSW005); Jiangsu Key Lab of Cancer Biomarkers, Prevention and Treatment, Collaborative Innovation Center for Cancer Personalized Medicine, Nanjing Medical University. We would like to thank Torsten Juelich for the professional language editing service.

Authors' contributions

Xu ZK and Wang LJ designed the study; Xia YW, Lv JL, Jiang TL and Li BW carried out the most experiments. Xuan Z and Sun GL performed bioinformatic analysis. Wang S conducted the statistical analysis. Xia YW wrote the manuscript, Li Z and Wang WZ revised the paper. All authors read and approved the final manuscript.

References

1. Bray F, Ferlay J, Soerjomataram I, Siegel RL, Torre LA, Jemal A. Global cancer statistics 2018: GLOBOCAN estimates of incidence and mortality worldwide for 36 cancers in 185 countries. CA Cancer J Clin. 2018; 68:394-424.
2. Clarke MF, Dick JE, Dirks PB, Eaves CJ, Jamieson CH, Jones DL, Visvader J, Weissman IL, Wahl GM. Cancer stem cells–perspectives on current status and future directions: AACR Workshop on cancer stem cells. Cancer Res. 2006; 66:9339-9344.
3. Beck B, Blanpain C. Unravelling cancer stem cell potential. Nat Rev Cancer. 2013; 13:727-738.
4. Xu G, Shen J, Ou YX, Sasahara M, Su X. Cancer stem cells: the 'heartbeat' of gastric cancer. J Gastroenterol. 2013; 48:781-797.
5. Takaishi S, Okumura T, Tu S, Wang SS, Shibata W, Vigneshwaran R, Gordon SA, Shimada Y, Wang TC. Identification of gastric cancer stem cells using the cell surface marker CD44. Stem Cells. 2009; 27:1006-1020.
6. Chen T, Yang K, Yu J, Meng W, Yuan D, Bi F, Liu F, Liu J, Dai B, Chen X, et al. Identification and expansion of cancer stem cells in tumor tissues and peripheral blood derived from gastric adenocarcinoma patients. Cell Res. 2012; 22:248-258.
7. Chen LL. The biogenesis and emerging roles of circular RNAs. Nat Rev Mol Cell Biol. 2016; 17:205-211.
8. Lasda E, Parker R. Circular RNAs: diversity of form and function. Rna. 2014; 20:1829-1842.
9. Sanger HL, Klotz G, Riesner D, Gross HJ, Kleinschmidt AK. Viroids are single-stranded covalently closed circular RNA molecules existing as highly base-paired rod-like structures. Proc Natl Acad Sci U S A. 1976; 73:3852-3856.
10. Cocquerelle C, Mascrez B, Hetuin D, Bailleul B. Mis-splicing yields circular RNA molecules. Faseb J. 1993; 7:155-160.

11. Capel B, Swain A, Nicolis S, Hacker A, Walter M, Koopman P, Goodfellow P, Lovell-Badge R. Circular transcripts of the testis-determining gene Sry in adult mouse testis. Cell. 1993; 73:1019-1030.
12. Enuka Y, Lauriola M, Feldman ME, Sas-Chen A, Ulitsky I, Yarden Y. Circular RNAs are long-lived and display only minimal early alterations in response to a growth factor. Nucleic Acids Res. 2016; 44:1370-1383.
13. Zhang Y, Xue W, Li X, Zhang J, Chen S, Zhang JL, Yang L, Chen LL. The Biogenesis of Nascent Circular RNAs. Cell Rep. 2016; 15:611-624.
14. Burd CE, Jeck WR, Liu Y, Sanoff HK, Wang Z, Sharpless NE. Expression of linear and novel circular forms of an INK4/ARF-associated non-coding RNA correlates with atherosclerosis risk. Plos Genet. 2010; 6:e1001233.
15. Memczak S, Jens M, Elefsinioti A, Torti F, Krueger J, Rybak A, Maier L, Mackowiak SD, Gregersen LH, Munschauer M, et al. Circular RNAs are a large class of animal RNAs with regulatory potency. Nature. 2013; 495:333-338.
16. Du WW, Yang W, Chen Y, Wu ZK, Foster FS, Yang Z, Li X, Yang BB. Foxo3 circular RNA promotes cardiac senescence by modulating multiple factors associated with stress and senescence responses. Eur Heart J. 2017; 38:1402-1412.
17. Hsiao KY, Lin YC, Gupta SK, Chang N, Yen L, Sun HS, Tsai SJ. Noncoding Effects of Circular RNA CCDC66 Promote Colon Cancer Growth and Metastasis. Cancer Res. 2017; 77:2339-2350.
18. Yu J, Xu Q, Wang Z, Yang Y, Zhang L, Ma J, Sun S, Yang F, Zhou W. Circular RNA cSMARCA5 inhibits growth and metastasis in hepatocellular carcinoma. J Hepatol. 2018; 68:1214-1227.
19. Han D, Li J, Wang H, Su X, Hou J, Gu Y, Qian C, Lin Y, Liu X, Huang M, et al. Circular RNA circMTO1 acts as the sponge of microRNA-9 to suppress hepatocellular carcinoma progression. Hepatology. 2017; 66:1151-1164.
20. Yu C, Li T, Wu Y, Yeh C, Chiang W, Chuang C, Kuo H. The circular RNA circBIRC6 participates in the molecular circuitry controlling human pluripotency. Nat Commun. 2017; 8.
21. Weng W, Wei Q, Toden S, Yoshida K, Nagasaka T, Fujiwara T, Cai S, Qin H, Ma Y, Goel A. Circular RNA ciRS-7-A Promising Prognostic Biomarker and a Potential Therapeutic Target in Colorectal Cancer. Clin Cancer Res. 2017; 23:3918-3928.
22. Li Y, Zheng Q, Bao C, Li S, Guo W, Zhao J, Chen D, Gu J, He X, Huang S. Circular RNA is enriched and stable in exosomes: a promising biomarker for cancer diagnosis. Cell Res. 2015; 25:981-984.
23. Jeck WR, Sharpless NE. Detecting and characterizing circular RNAs. Nat Biotechnol. 2014; 32:453-461.
24. Li B, Wang W, Li Z, Chen Z, Zhi X, Xu J, Li Q, Wang L, Huang X, Wang L, et al. MicroRNA-148a-3p enhances cisplatin cytotoxicity in gastric cancer through mitochondrial fission induction and cyto-protective autophagy suppression. Cancer Lett. 2017; 410:212-227.
25. Hammond SM, Sharpless NE. HMGA2, microRNAs, and stem cell aging. Cell. 2008; 135:1013-1016.

26. Fedele M, Visone R, De Martino I, Troncone G, Palmieri D, Battista S, Ciarmiello A, Pallante P, Arra C, Melillo RM, et al. HMGA2 induces pituitary tumorigenesis by enhancing E2F1 activity. Cancer Cell. 2006; 9:459-471.
27. Busch B, Bley N, Muller S, Glass M, Misiak D, Lederer M, Vetter M, Strauss HG, Thomssen C, Huttelmaier S. The oncogenic triangle of HMGA2, LIN28B and IGF2BP1 antagonizes tumor-suppressive actions of the let-7 family. Nucleic Acids Res. 2016; 44:3845-3864.
28. Huang B, Yang J, Cheng Q, Xu P, Wang J, Zhang Z, Fan W, Wang P, Yu M. Prognostic Value of HMGA2 in Human Cancers: A Meta-Analysis Based on Literatures and TCGA Datasets. Front Physiol. 2018; 9:776.
29. Liang D, Tatomer DC, Luo Z, Wu H, Yang L, Chen LL, Cherry S, Wilusz JE. The Output of Protein-Coding Genes Shifts to Circular RNAs When the Pre-mRNA Processing Machinery Is Limiting. Mol Cell. 2017; 68:940-954.
30. Conn SJ, Pillman KA, Toubia J, Conn VM, Salmanidis M, Phillips CA, Roslan S, Schreiber AW, Gregory PA, Goodall GJ. The RNA binding protein quaking regulates formation of circRNAs. Cell. 2015; 160:1125-1134.
31. Bailey TL, Boden M, Buske FA, Frith M, Grant CE, Clementi L, Ren J, Li WW, Noble WS. MEME SUITE: tools for motif discovery and searching. Nucleic Acids Res. 2009; 37:W202-W208.
32. Fei T, Chen Y, Xiao T, Li W, Cato L, Zhang P, Cotter MB, Bowden M, Lis RT, Zhao SG, et al. Genome-wide CRISPR screen identifies HNRNPL as a prostate cancer dependency regulating RNA splicing. Proc Natl Acad Sci U S A. 2017; 114:E5207-E5215.
33. Vermeulen L, Melo FDSE, Richel DJ, Medema JP. The developing cancer stem-cell model: clinical challenges and opportunities. Lancet Oncol. 2012; 13:e83-e89.
34. Li X, Yang L, Chen LL. The Biogenesis, Functions, and Challenges of Circular RNAs. Mol Cell. 2018; 71:428-442.
35. Salmena L, Poliseno L, Tay Y, Kats L, Pandolfi PP. A ceRNA hypothesis: the Rosetta Stone of a hidden RNA language? Cell. 2011; 146:353-358.
36. Bianchi ME, Agresti A. HMG proteins: dynamic players in gene regulation and differentiation. Curr Opin Genet Dev. 2005; 15:496-506.
37. Nishino J, Kim I, Chada K, Morrison SJ. Hmga2 promotes neural stem cell self-renewal in young but not old mice by reducing p16Ink4a and p19Arf Expression. Cell. 2008; 135:227-239.
38. Chieffi P, Battista S, Barchi M, Di Agostino S, Pierantoni GM, Fedele M, Chiariotti L, Tramontano D, Fusco A. HMGA1 and HMGA2 protein expression in mouse spermatogenesis. Oncogene. 2002; 21:3644-3650.
39. Dong J, Wang R, Ren G, Li X, Wang J, Sun Y, Liang J, Nie Y, Wu K, Feng B, et al. HMGA2-FOXL2 Axis Regulates Metastases and Epithelial-to-Mesenchymal Transition of Chemoresistant Gastric Cancer. Clin Cancer Res. 2017; 23:3461-3473.
40. Sun J, Sun B, Zhu D, Zhao X, Zhang Y, Dong X, Che N, Li J, Liu F, Zhao N, et al. HMGA2 regulates CD44 expression to promote gastric cancer cell motility and sphere formation. Am J Cancer Res.

2017; 7:260-274.

41. Schoenmakers EF, Wanschura S, Mols R, Bullerdiek J, Van den Berghe H, Van de Ven WJ. Recurrent rearrangements in the high mobility group protein gene, HMGI-C, in benign mesenchymal tumours. Nat Genet. 1995; 10:436.
42. Chen RX, Chen X, Xia LP, Zhang JX, Pan ZZ, Ma XD, Han K, Chen JW, Judde JG, Deas O, et al. N(6)-methyladenosine modification of circNSUN2 facilitates cytoplasmic export and stabilizes HMGA2 to promote colorectal liver metastasis. Nat Commun. 2019; 10:4695.
43. Shan K, Liu C, Liu B, Chen X, Dong R, Liu X, Zhang Y, Liu B, Zhang S, Wang J, et al. Circular Noncoding RNA HIPK3 Mediates Retinal Vascular Dysfunction in Diabetes Mellitus. Circulation. 2017; 136:1629-1642.
44. Zeng K, Chen X, Xu M, Liu X, Hu X, Xu T, Sun H, Pan Y, He B, Wang S. CircHIPK3 promotes colorectal cancer growth and metastasis by sponging miR-7. Cell Death Dis. 2018; 9.
45. Meng J, Chen S, Han JX, Qian B, Wang XR, Zhong WL, Qin Y, Zhang H, Gao WF, Lei YY, et al. Twist1 Regulates Vimentin through Cul2 Circular RNA to Promote EMT in Hepatocellular Carcinoma. Cancer Res. 2018; 78:4150-4162.
46. Wikonkal NM, Remenyik E, Knezevic D, Zhang W, Liu M, Zhao H, Berton TR, Johnson DG, Brash DE. Inactivating E2f1 reverts apoptosis resistance and cancer sensitivity in Trp53-deficient mice. Nat Cell Biol. 2003; 5:655-660.
47. Dick FA, Dyson N. pRB contains an E2F1-specific binding domain that allows E2F1-induced apoptosis to be regulated separately from other E2F activities. Mol Cell. 2003; 12:639-649.
48. Ashwal-Fluss R, Meyer M, Pamudurti NR, Ivanov A, Bartok O, Hanan M, Evantal N, Memczak S, Rajewsky N, Kadener S. circRNA biogenesis competes with pre-mRNA splicing. Mol Cell. 2014; 56:55-66.
49. Pagliarini V, Jolly A, Bielli P, Di Rosa V, De la Grange P, Sette C. Sam68 binds Alu-rich introns in SMN and promotes pre-mRNA circularization. Nucleic Acids Res. 2019.
50. Geuens T, Bouhy D, Timmerman V. The hnRNP family: insights into their role in health and disease. Hum Genet. 2016; 135:851-867.
51. Gallardo M, Hornbaker MJ, Zhang X, Hu P, Bueso-Ramos C, Post SM. Aberrant hnRNP K expression: All roads lead to cancer. Cell Cycle. 2016; 15:1552-1557.
52. Li D, Wang X, Mei H, Fang E, Ye L, Song H, Yang F, Li H, Huang K, Zheng L, et al. Long Noncoding RNA pancEts-1 Promotes Neuroblastoma Progression through hnRNPK-Mediated β-Catenin Stabilization. Cancer Res. 2018; 78:1169-1183.
53. Zhang Z, Zhou C, Chang Y, Zhang Z, Hu Y, Zhang F, Lu Y, Zheng L, Zhang W, Li X, et al. Long non-coding RNA CASC11 interacts with hnRNP-K and activates the WNT/β-catenin pathway to promote growth and metastasis in colorectal cancer. Cancer Lett. 2016; 376:62-73.

Figures

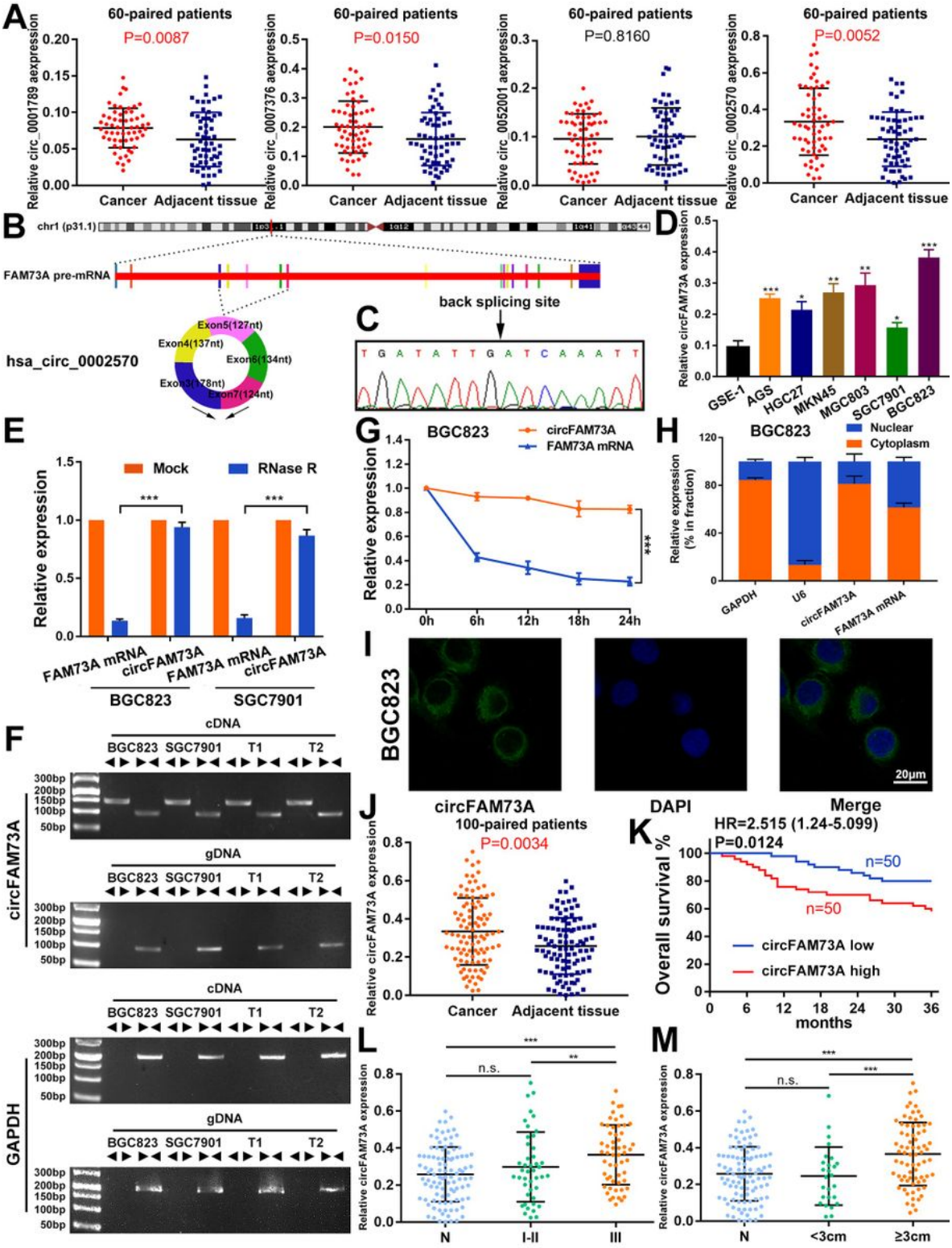

Figure 1

CircFAM73A is upregulated in GC and high circFAM73A predicts poor prognosis (A) Validated the expression of hsa_circ_0001789, hsa_circ_0007376, hsa_circ_0052001 and hsa_circ_0002570 in the 60 paired GC and adjacent tissues by qRT-PCR. (B) Schematic drawing illustrating circFAM73A (hsa_circ_0002570) (700 bp) arose from exon 3,4,5,6,7 of the FAM73A gene. (C) Arrow represents the "head-to-tail" splicing sites of circFAM73A confirmed by Sanger sequencing. (D) Relative circFAM73A

expression in 6 GC cell lines relative to normal human gastric epithelial cell line GES-1. (E) qRT-PCR analysis of the level of circFAM73A and linear FAM73A mRNA after treatment with RNase R in BGC823 and SGC7901 (normalized to mock treatment). (F) The existence of circFAM73A was validated in BGC823 and SGC7901 and two GC samples (T1 and T2) by RT-PCR. Divergent primers amplified circFAM73A from cDNA, but not from genomic DNA (gDNA). GAPDH was used as a negative control. (G) Relative levels of circFAM73A and FAM73A mRNA were measured by qRT-PCR in BGC823 treated with Actinomycin D for different periods of time. (H) Relative levels of GAPDH (positive control for cytoplasmic fraction), U6 (positive control for nuclear fraction), circFAM73A and FAM73A mRNA from nuclear and cytoplasmic fractions in BGC823. (I) Fluorescence in situ hybridization (FISH) was conducted to determine the subcellular localization of circFAM73A in BGC823. DAPI was used for nuclei staining. Scale bar: 20 μm. (J) Relative circFAM73A expression in additional 100 paired GC and adjacent tissues. (K) Overall survival analysis based on circFAM73A expression in 100 GC patients. The median circFAM73A expression is used as a cutoff. (L) The association of circFAM73A expression and TMN stage through qRT-PCR. (M) The association of circFAM73A expression and tumor size through qRT-PCR. Graph represents mean ± SD; *$p < 0.05$, **$p < 0.01$, and ***$p < 0.001$.

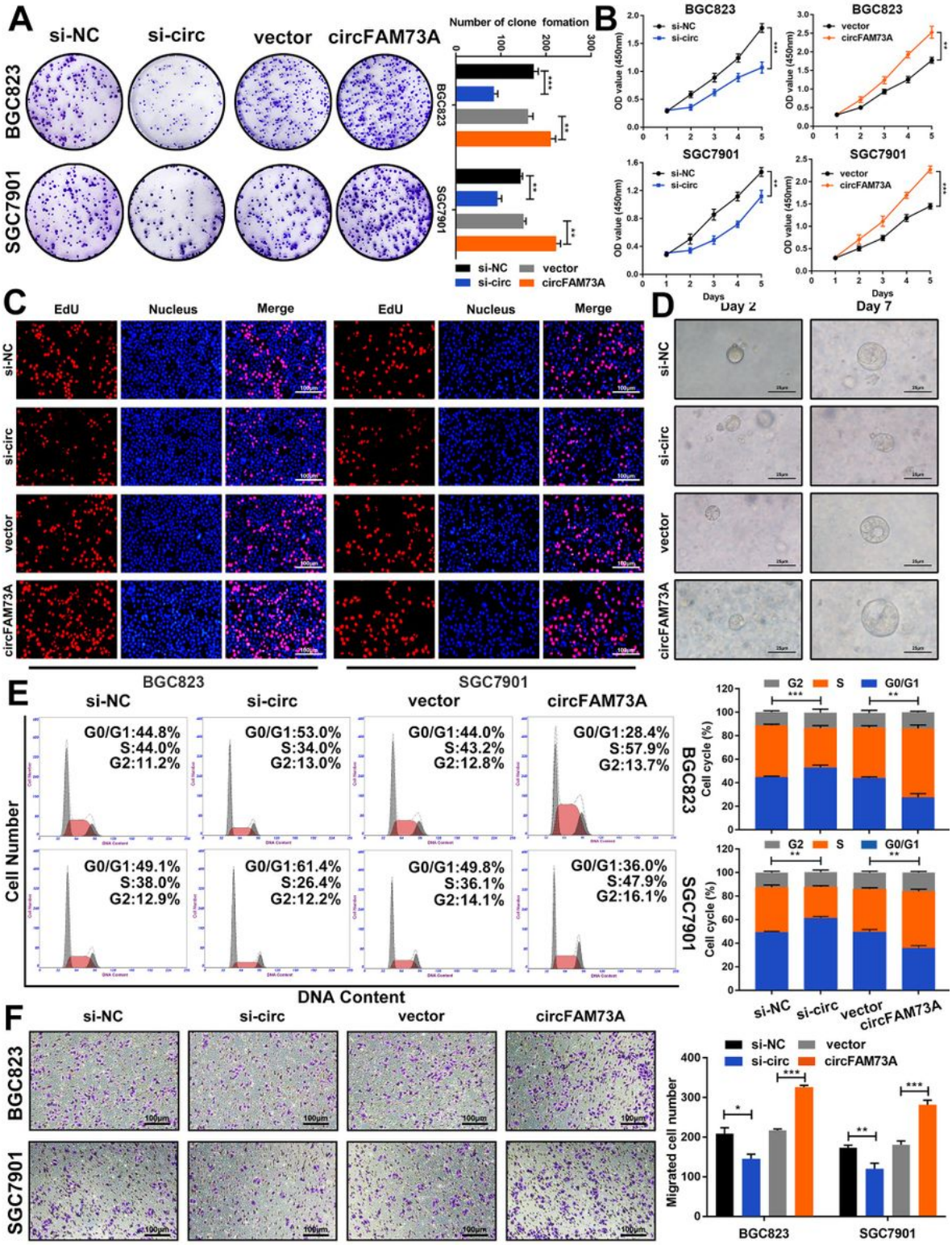

Figure 2

CircFAM73A promotes the proliferation and migration of GC in vitro (A) Colony formation assay of BGC823 and SGC7901 transfected with control, circFAM73A siRNA, vector or circFAM73A plasmid. (B, C) CCK-8 and EdU assays were performed to evaluate cell proliferative effects of circFAM73A in BGC823 and SGC7901. Scale bar: 100 μm. (D) Effects of circFAM73A alteration on the growth of gastric organoids. Scale bar: 25 μm. (E) Effects of circFAM73A alteration on cell cycle distribution of BGC823

and SGC7901 detected by flow cytometry. (F) Effects of circFAM73A alteration on cell migration ability were tested by Transwell assay. Scale bar: 100 μm. Graph represents mean ± SD; *p < 0.05, **p < 0.01, ***p < 0.001.

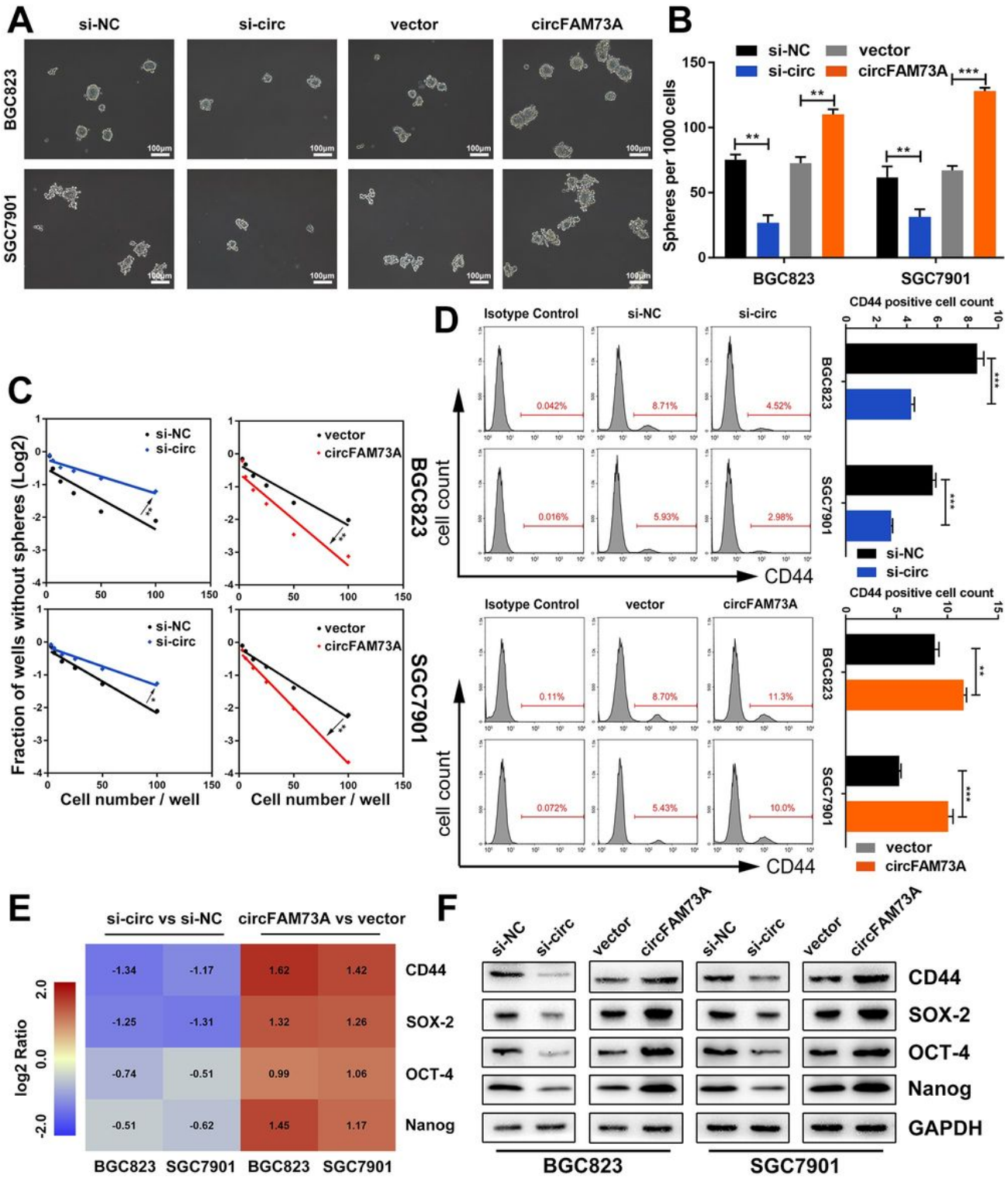

Figure 3

CircFAM73A enhances the stem cell-like property in GC cells (A) Representative images of formatted spheres among indicated cells. Scale bar: 100 μm. (B) Sphere formation abilities were accessed by the

number of spheres. (C) Effects of circFAM73A alteration on capacity of sphere formation were measured by extreme limiting dilution assay. (D) Representative flow cytometric histograms and quantification of the CD44 positive proportion among indicated cells. (E) Several stemness-related factors including CD44, SOX-2, OCT-4 and Nanog were measured by qRT-PCR. Pseudocolors represent the intensity scale of expression in circFAM73A vs. vector cells and si-circFAM73A vs. control cells calculated by log2 transformation. (F) Western blot of stemness-related factors including CD44, SOX-2, OCT-4 and Nanog among indicated cells. Graph represents mean ± SD; *p < 0.05, **p < 0.01, ***p < 0.001.

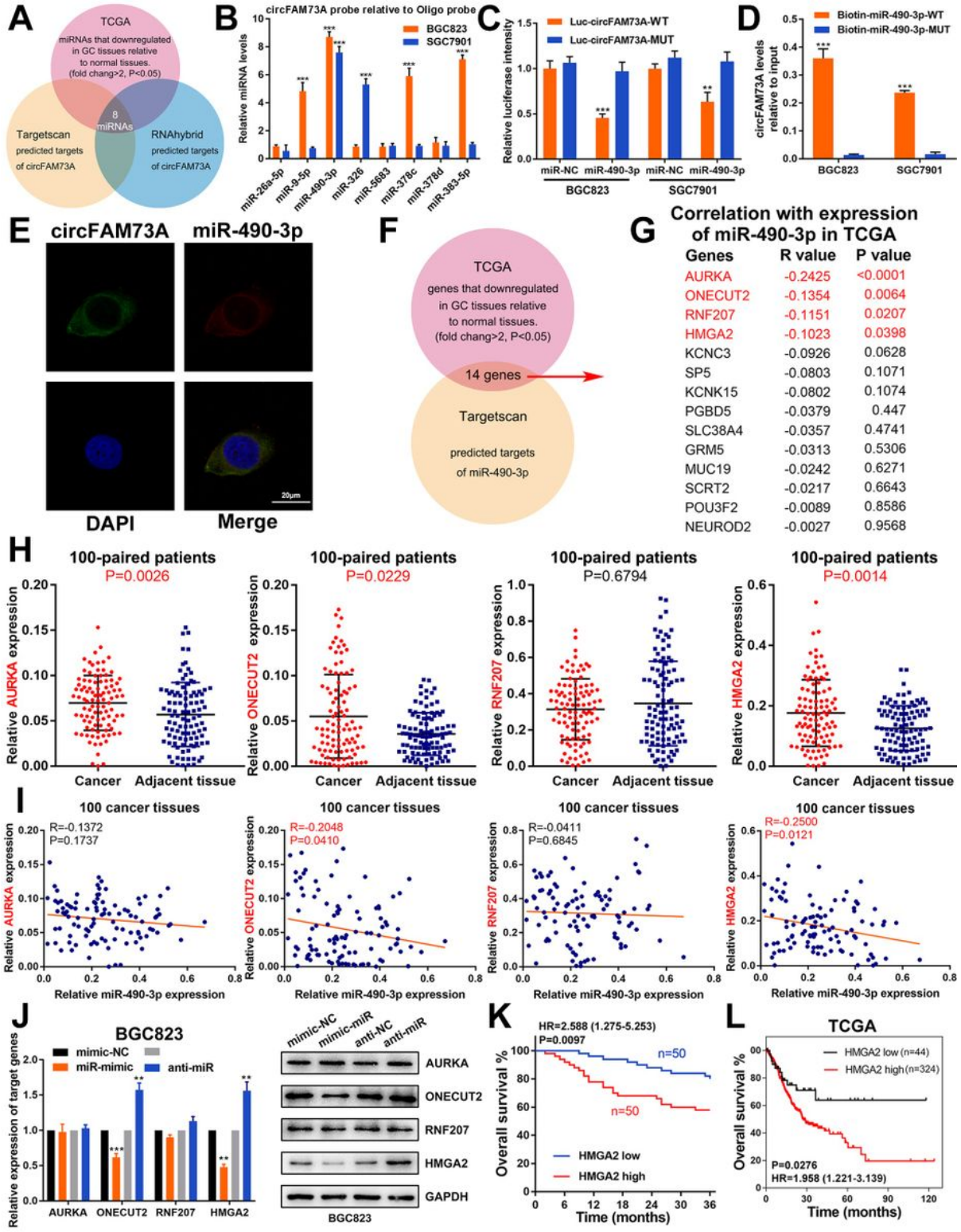

Figure 4

CircFAM73A acts as a sponge of miR-490-3p, HMGA2 is the direct downstream target of miR-490-3p (A) Venn diagram showing the overlap of target miRNAs of circFAM73A predicted by TargetScan and RNAhybrid and downregulated miRNAs in GC from TCGA. (B) The expression levels of 8 miRNAs candidate miRNAs were quantified by qRT-PCR after pull-down with biotin-labeled circFAM73A probe in BGC823 and SGC7901 cells. (C) Luciferase intensity in BGC823 and SGC7901 cells co-transfected with luciferase reporter containing with wild-type or mutated circFAM73A-miR-490-3p binding sequences and the mimics of miR-490-3p or control. (D) The expression levels of circFAM73A were tested by qRT-PCR after pull-down with biotin-labeled wild-type or mutant miR-490-3p in circFAM73A overexpressed BGC823 and SGC7901 cells. (E) Fluorescence in situ hybridization assay revealed the co-location between circFAM73A and miR-490-3p in cytoplasm. Scare bar = 20 μm. (F, G) Venn diagram detailing the exploration of miR-490-3p downstream targets. (H) The mRNA expression of AURKA, ONECUT2, RNF207 and HMGA2 in 100 paired GC and adjacent tissues were determined by qRT-PCR. (I) Correlation between miR-490-3p and AURKA, ONECUT2, RNF207 and HMGA2 according to our GC samples. (J) The expression of AURKA, ONECUT2, RNF207 and HMGA2 after miR-490-3p alternation in BGC823 cells measured by qRT-PCR and Western Blot. (K) Overall survival analysis based on HMGA2 expression in 100 GC patients. The median HMGA2 expression is used as a cutoff. (L) Overall survival analysis based on HMGA2 expression in TCGA GC patients. The optimal cut-off was calculated by X-tile software. Graph represents mean ± SD; *$p < 0.05$, **$p < 0.01$, ***$p < 0.001$.

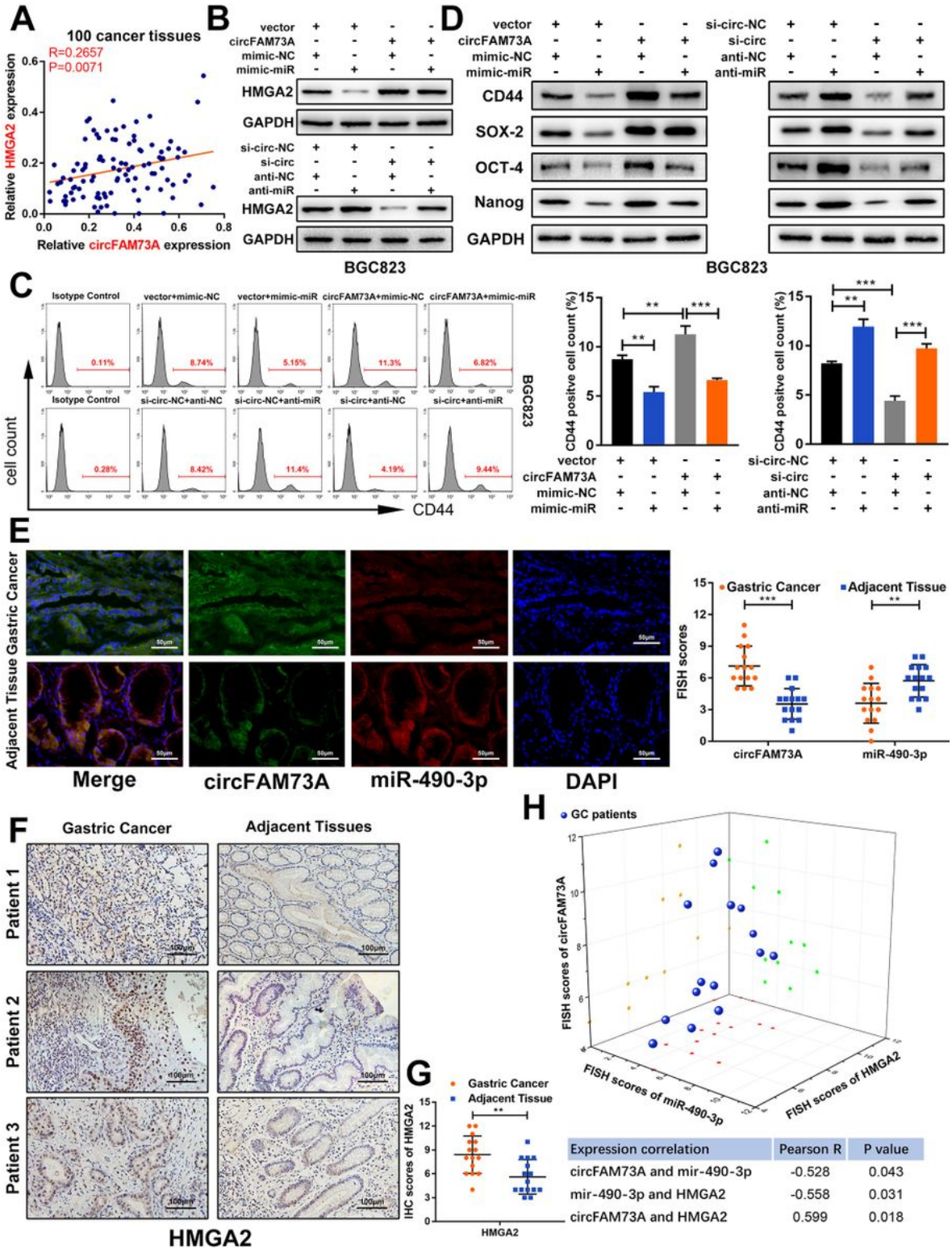

Expression correlation	Pearson R	P value
circFAM73A and mir-490-3p	-0.528	0.043
mir-490-3p and HMGA2	-0.558	0.031
circFAM73A and HMGA2	0.599	0.018

Figure 5

CircFAM73A regulates HMGA2 expression by miR-490-3p (A) Correlation between circFAM73A and HMGA2 according to our GC samples. (B) Western blot of HMGA2 was detected in BGC823 transfected with indicated vectors. (C) Representative flow cytometric histograms and quantification of the CD44 positive proportion in BGC823 transfected with indicated vectors. (D) Western blot of stemness-related factors including CD44, SOX-2, OCT-4 and Nanog in BGC823 transfected with indicated vectors. (E) FISH

assay of circFAM73A and miR-490-3p in 15 paired GC and adjacent tissues from patients. FISH scores were further assessed. Nuclei were stained with DAPI. Scale bar: 50 μm. (F) IHC staining of HMGA2 in in 15 paired GC and adjacent tissues. Scale bar: 100 μm. (G) The IHC scores of HMGA2 were further quantified. (H) Three-dimensional scatter plot of circFAM73A, miR-490-3p and HMGA2 15 paired GC and adjacent tissues. Graph represents mean ± SD; *p < 0.05, **p < 0.01, ***p < 0.001.

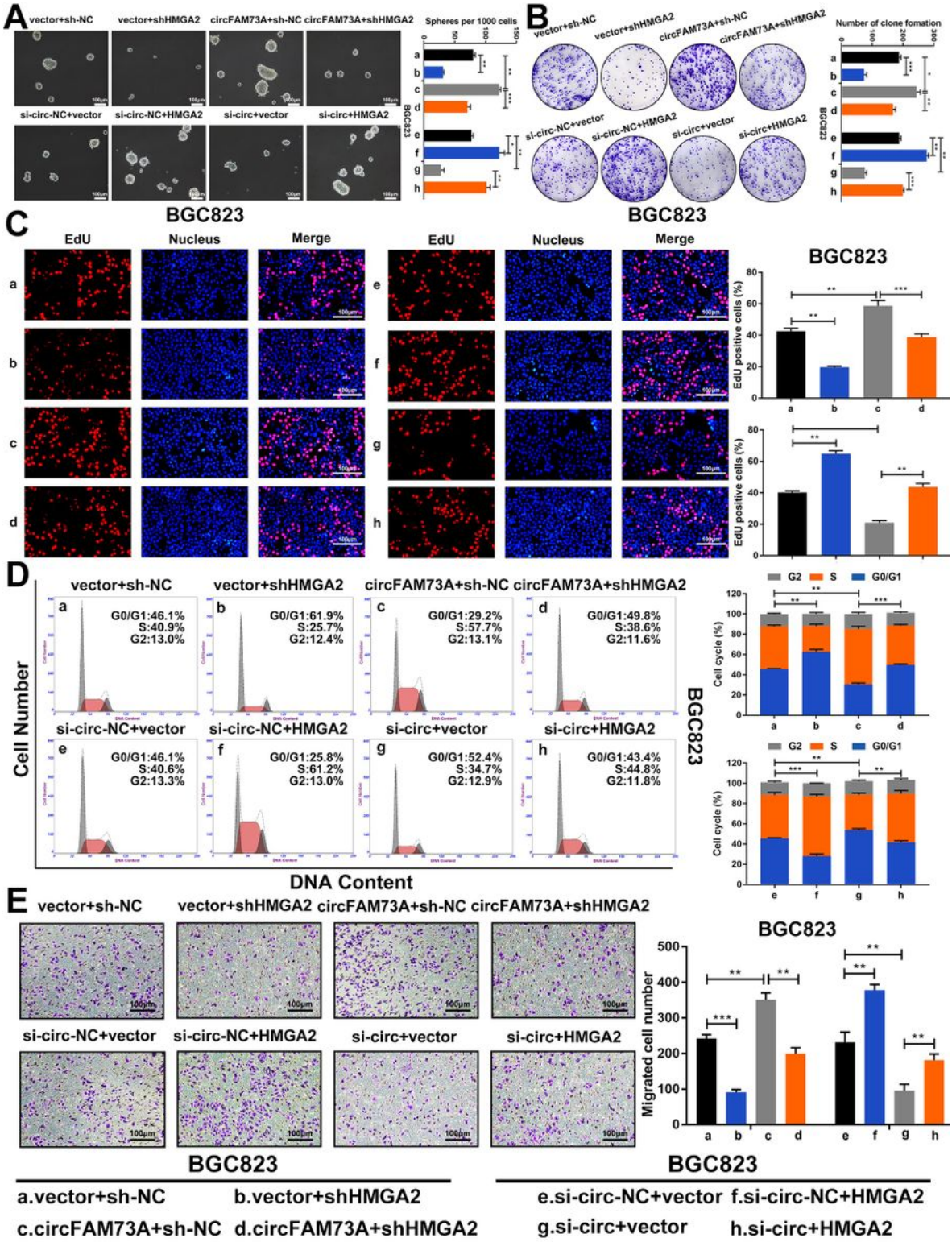

Figure 6

CircFAM73A promotes stem cell-like property and cell malignancy in GC cells by upregulating HMGA2 expression (A) Representative images of and quantification of formatted spheres among indicated cells. Scale bar: 100 μm. (B, C) Colony formation assay and EdU assays were performed to assess cell proliferative effects. Scale bar: 100 μm. (E) Cell cycle distribution was detected by flow cytometry. (F) Cell migration ability were tested by Transwell assay. Scale bar: 100 μm. Graph represents mean ± SD; *p < 0.05, **p < 0.01, ***p < 0.001.

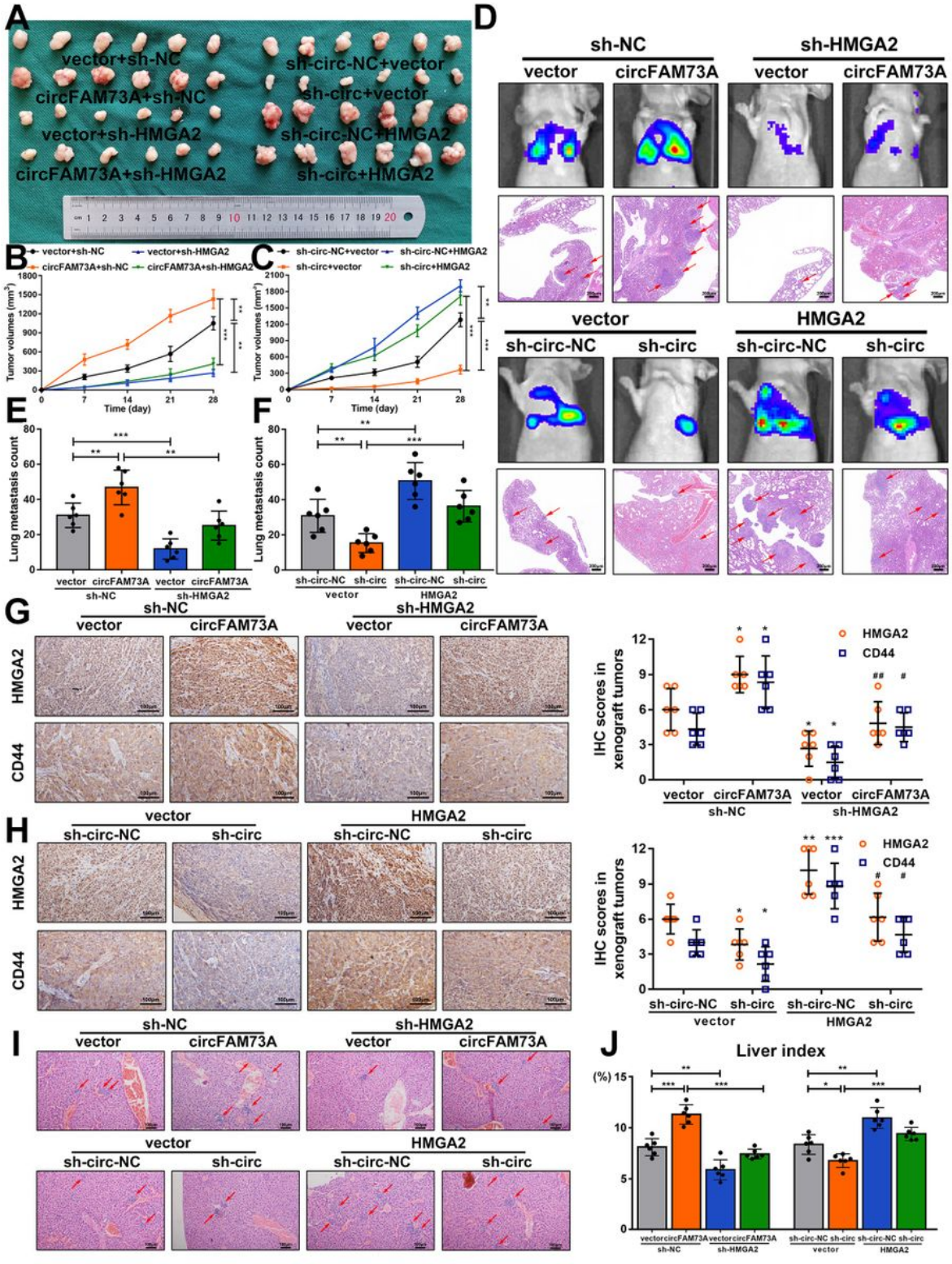

Figure 7

CircFAM73A regulates HMGA2 expression level to promote GC growth and metastasis in vivo (A) The images of xenograft tumors of sacrificed mice subcutaneous injected with indicated cells 4 weeks after injections. (B, C) Growth curves of xenograft tumors. Tumor volume was calculated by 1/2 (length × width2). (D) Representative images of bioluminescent images of mice by IVIS Imaging system and HE staining of lung tissues. Scale bar: 200 μm. (E) Quantification of metastatic foci in mice lungs injected with indicated cells. (G, H) Immunohistochemistry staining and IHC scores of HMGA2 and CD44 in respective xenograft tumor tissues. * vs the group of first column, # vs the group of second column. (I) Representative images of HE staining of liver tissues from mice with portal veins injection. Scale bar: 100 μm. (J) Liver indexes (liver weight/ body weight) of each group were calculated. Graph represents mean ± SD; *p < 0.05, **p < 0.01, ***p < 0.001, #p < 0.05, # #p < 0.01, # # #p < 0.001.

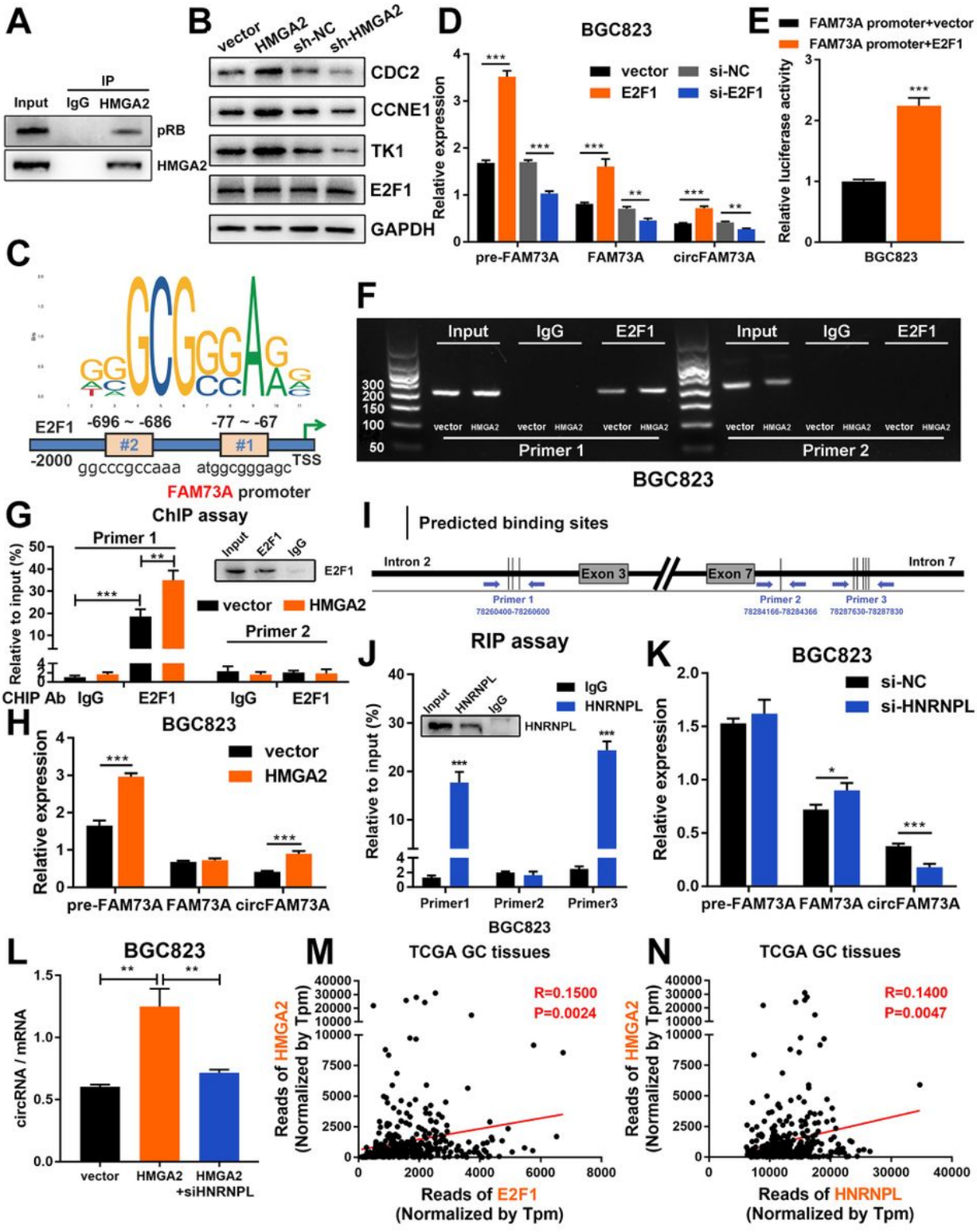

Figure 8

HMGA2 elevates circFAM73A expression reciprocally by E2F1 and HNRNPL (A) Co-immunoprecipitation was performed using control IgG or HMGA2 antibody. Immunoprecipitated proteins were detected by pRB and HMGA2 antibodies. (B) Western blot of E2F1 and classical E2F1 responsive effectors (CCNE1, TK1 and CDC2) in BGC823. (C) Putative binding sites of E2F1 in FAM73A promoter region predicted by JASPAR. (D) Relative expression of pre-FAM73A, FAM73A mRNA and circFAM73A with E2F1 alteration

were measured by qRT-PCR in BGC823. (E) Luciferase reporter assay analysis of FAM73A promoter luciferase reporters in BGC823 cells transfected with E2F1 or control. (F) RT-PCR was performed in BGC823 cells after chromatin immunoprecipitation by E2F1 antibody or control IgG and by two pairs of primers to validate the E2F1 binding sites in FAM73A promoter region. (G) qRT-PCR analysis of chromatin immunoprecipitation assay in E. (H) Relative expression of pre-FAM73A, FAM73A mRNA and circFAM73A in BGC823 with HMGA2 reconstitution were measured by qRT-PCR. (I) Schematic diagram demonstrated three designed specific primers covering different binding site sequences in intron-2 and intron-7. (J) Relative enrichment of amplification sequence by three indicated primes after RNA binding protein immunoprecipitation assay by HNRNPL antibody or control IgG in BGC823. (K) Relative expression of pre-FAM73A, FAM73A mRNA and circFAM73A in BGC823 with HNRNPL suppression were measured by qRT-PCR. (L) The ratio of circFAM73A expression to FAM73A mRNA expression in BGC823. (M) Correlation between E2F1 and HMGA2 according to TCGA statistics. (N) Correlation between HNRNPL and HMGA2 according to TCGA statistics. Graph represents mean ± SD; *$p < 0.05$, **$p < 0.01$, ***$p < 0.001$.

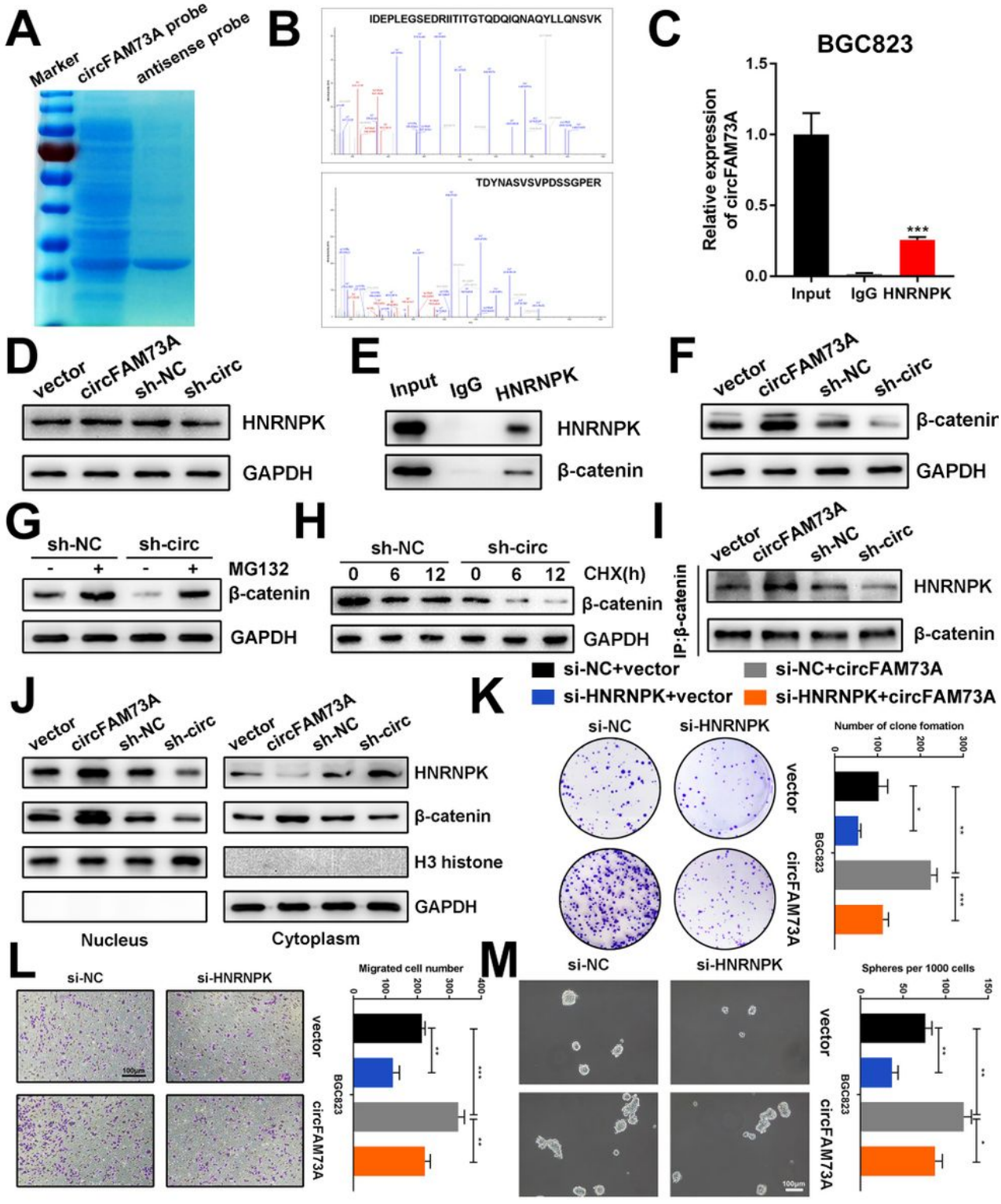

Figure 9

CircFAM73A interacts with HNRNPK and facilitates β-catenin stabilization (A) Coomassie blue staining of circFAM73A pulldown. (B) Spectra of HNRNPK identified by mass spectrometry. (C) Relative abundance of circFAM73A detected by qRT-PCR after RIP using HNRNPK antibody in BGC823. (D) Expression of HNRNPK protein of BGC823 after circFAM73A overexpression or knocking-down measured by Western Blot. (E) Co-IP analysis using HNRNPK protein revealing the endogenous interaction between HNRNPK

and β-catenin in BGC823. (F) Expression of β-catenin protein in BGC823 after circFAM73A overexpression or knocking-down measured by Western Blot. (G) Expression of β-catenin protein in BGC823 transfected with control shRNA or sh-circFAM73A and treated with MG132 (10 μmol/L, 10 h) or untreated measured by Western Blot. (H) Expression of β-catenin protein in BGC823 transfected with control shRNA or sh-circFAM73A and treated with cycloheximide (CHX, 50 μg/mL) for different time measured by Western Blot. (I) Co-IP and Western blot showing the interaction between HNRNPK and β-catenin after circFAM73A overexpression or knocking-down in BGC823. (J) The nuclear and cytoplasmic expression of HNRNPK and β-catenin measured by Western Blot after circFAM73A overexpression or knocking-down in BGC823. (K-M) Representative images of and quantification of clone formation (K) migrated cells (L) and formatted spheres (M) in BGC823 transfected with vector or circFAM73A plasmid and co-transfected with control siRNA or si-HNRNPK. Graph represents mean ± SD; *p < 0.05, **p < 0.01, ***p < 0.001.

Supplementary Files

This is a list of supplementary files associated with this preprint. Click to download.

- SupplementaryFigureLegdend.docx
- SupplementaryTable.docx
- supFigure1.tif
- supFigure2.tif
- supFigure3.tif
- supFigure4.tif
- supFigure5.tif
- supFigure6.tif
- supFigure7.tif
- supFigure8.tif
- supFigure9.tif